Designation: E2899 – 15

Standard Test Method for Measurement of Initiation Toughness in Surface Cracks Under Tension and Bending[1]

This standard is issued under the fixed designation E2899; the number immediately following the designation indicates the year of original adoption or, in the case of revision, the year of last revision. A number in parentheses indicates the year of last reapproval. A superscript epsilon (ε) indicates an editorial change since the last revision or reapproval.

1. Scope

1.1 This test method describes the method for testing fatigue-sharpened, semi-elliptically shaped surface cracks in rectangular flat panels subjected to monotonically increasing tension or bending. Tests quantify the crack-tip conditions at initiation of stable crack extension or immediate unstable crack extension.

1.2 This test method applies to the testing of metallic materials not limited by strength, thickness, or toughness. Materials are assumed to be essentially homogeneous and free of residual stress. Tests may be conducted at any appropriate temperature. The effects of environmental factors and sustained or cyclic loads are not addressed in this test method.

1.3 This test method describes all necessary details for the user to test for the initiation of crack extension in surface crack test specimens. Specific requirements and recommendations are provided for test equipment, instrumentation, test specimen design, and test procedures.

1.4 Tests of surface cracked, laboratory-scale specimens as described in this test method may provide a more accurate understanding of full-scale structural performance in the presence of surface cracks. The provided recommendations help to assure test methods and data are applicable to the intended purpose.

1.5 This test method prescribes a consistent methodology for test and analysis of surface cracks for research purposes and to assist in structural assessments. The methods described here utilize a constraint-based framework (**1, 2**)[2] to evaluate the fracture behavior of surface cracks.

NOTE 1—*Constraint-based framework*. In the context of this test method, constraint is used as a descriptor of the three-dimensional stress and strain fields in the near vicinity of the crack tip, where material contractions due to the Poisson effect may be suppressed and therefore produce an elevated, tensile stress state (**3, 4**). (See further discussions in Terminology and Significance and Use.) When a parameter describing this stress state, or constraint, is used with the standard measure of crack-tip stress amplitude (K or J), the resulting two-parameter characterization broadens the ability of fracture mechanics to accurately predict the response of a crack under a wider range of loading. The two-parameter methodology produces a more complete description of the crack-tip conditions at the initiation of crack extension. The effects of constraint on measured fracture toughness are material dependent and are governed by the effects of the crack-tip stress-strain state on the micromechanical failure processes specific to the material. Surface crack tests conducted with this test method can help to quantify the material sensitivity to constraint effects and to establish the degree to which the material toughness correlates with a constraint-based fracture characterization.

1.6 This test method provides a quantitative framework to categorize test specimen conditions into one of three regimes: (I) a linear-elastic regime, (II) an elastic-plastic regime, or (III) a field-collapse regime. Based on this categorization, analysis techniques and guidelines are provided to determine an applicable crack-tip parameter for the linear-elastic regime (K or J) or the elastic-plastic regime (J), and an associated constraint parameter. Recommendations are provided to assess the test data in the context of a toughness-constraint locus (**2**). The user is directed to other resources for evaluation of the test specimen in the field-collapse regime when extensive plastic deformation in the specimen eliminates the identifiable crack-front fields of fracture mechanics.

1.7 The specimen design and test procedures described in this test method may be applied to evaluation of surface cracks in welds; however, the methods described in this test method to analyze test measurements may not be applicable. Weld fracture tests generally have complicating features beyond the scope of data analysis in this test method, including the effects of residual stress, microstructural variability, and non-uniform strength. These effects will influence test results and must be considered in the interpretation of measured quantities.

1.8 This test method is not intended for testing surface cracks in steel in the cleavage regime. Such tests are outside the scope of this test method. A methodology for evaluation of cleavage fracture toughness in ferritic steels over the ductile-to-brittle region using C(T) and SE(B) specimens can be found in Test Method E1921.

1.9 *Units*—The values stated in SI units are to be regarded as the standard. The values given in parentheses are for information only.

[1] This test method is under the jurisdiction of ASTM Committee E08 on Fatigue and Fracture and is the direct responsibility of Subcommittee E08.07 on Fracture Mechanics.

Current edition approved June 1, 2015. Published August 2015. Last previous edition approved in 2013 as E2899 – 13. DOI: 10.1520/E2899-15.

[2] The boldface numbers in parentheses refer to the list of references at the end of this test method.

1.10 This practice may involve hazardous materials, operations, and equipment. *This standard does not purport to address all of the safety problems associated with its use. It is the responsibility of the users of this standard to establish appropriate safety and health practices and to determine the applicability of regulatory limitations prior to use.*

2. Referenced Documents

2.1 *ASTM Standards:*[3]

C1421 Test Methods for Determination of Fracture Toughness of Advanced Ceramics at Ambient Temperature

E4 Practices for Force Verification of Testing Machines

E6 Terminology Relating to Methods of Mechanical Testing

E8/E8M Test Methods for Tension Testing of Metallic Materials

E111 Test Method for Young's Modulus, Tangent Modulus, and Chord Modulus

E399 Test Method for Linear-Elastic Plane-Strain Fracture Toughness K_{Ic} of Metallic Materials

E647 Test Method for Measurement of Fatigue Crack Growth Rates

E740 Practice for Fracture Testing with Surface-Crack Tension Specimens

E1012 Practice for Verification of Testing Frame and Specimen Alignment Under Tensile and Compressive Axial Force Application

E1820 Test Method for Measurement of Fracture Toughness

E1823 Terminology Relating to Fatigue and Fracture Testing

E1921 Test Method for Determination of Reference Temperature, T_o, for Ferritic Steels in the Transition Range

[3] For referenced ASTM standards, visit the ASTM website, www.astm.org, or contact ASTM Customer Service at service@astm.org. For *Annual Book of ASTM Standards* volume information, refer to the standard's Document Summary page on the ASTM website.

3. Terminology

3.1 For definitions of terms used in this Test Method, Terminologies E6 and E1823 apply.

3.2 *Symbols:*

3.2.1 *crack depth, a [L]*—see Terminology E1823 and Fig. 1 in this test method.

3.2.1.1 *Discussion*—In this test method, the term a_o is the original surface crack depth, as determined in subsection 8.4, used in the evaluation of the test.

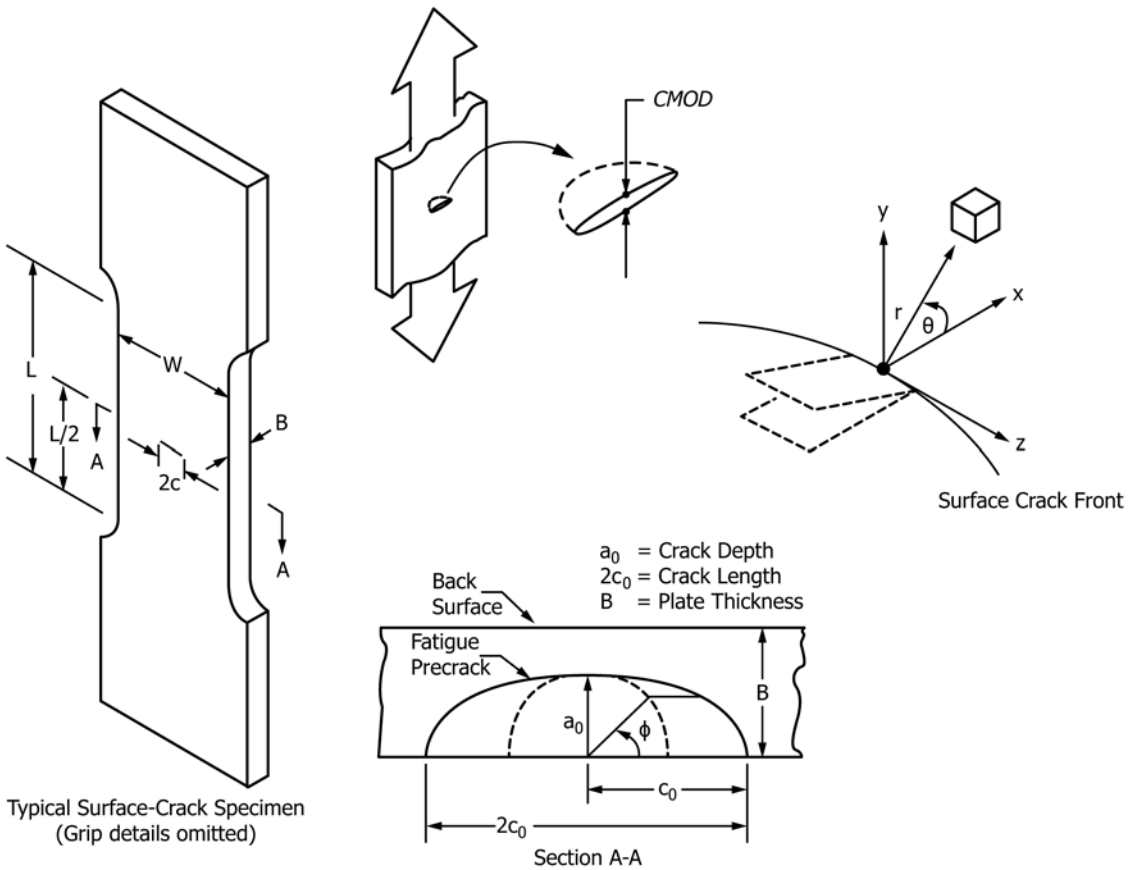

FIG. 1 Test Specimen and Crack Configurations

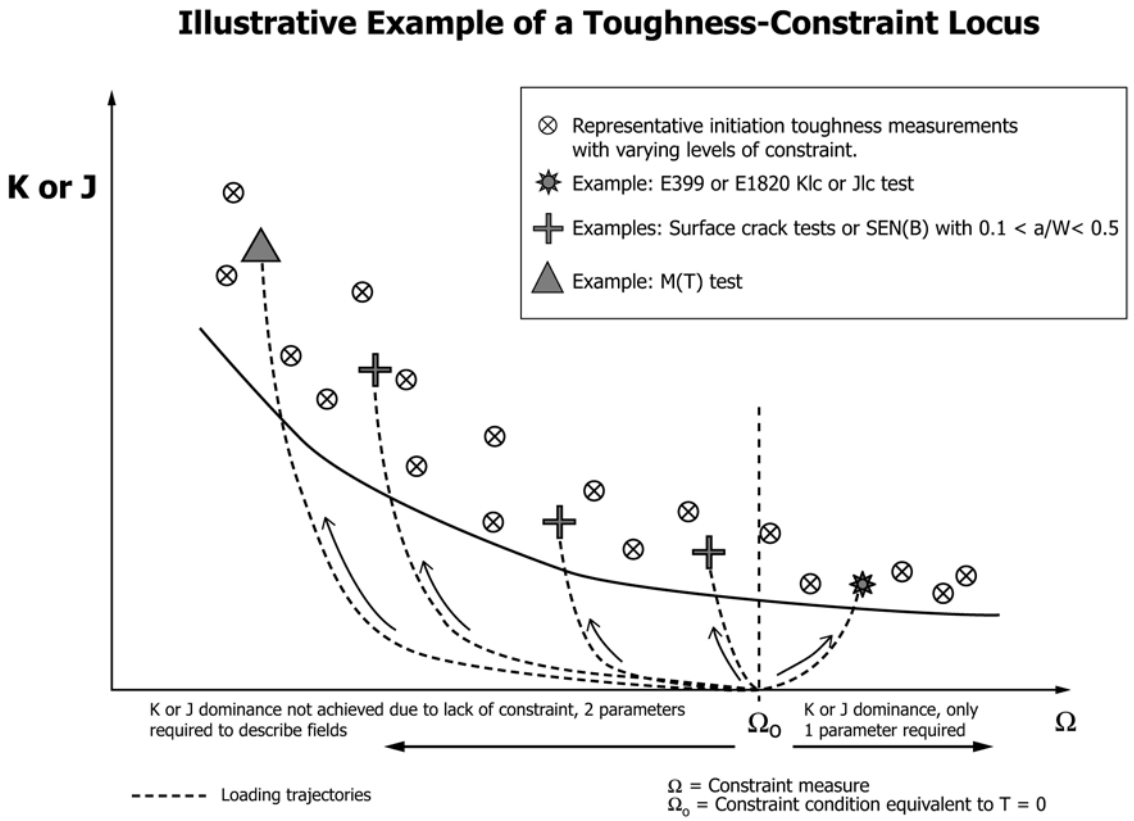

FIG. 2 Toughness-Constraint Locus with Example Trajectories

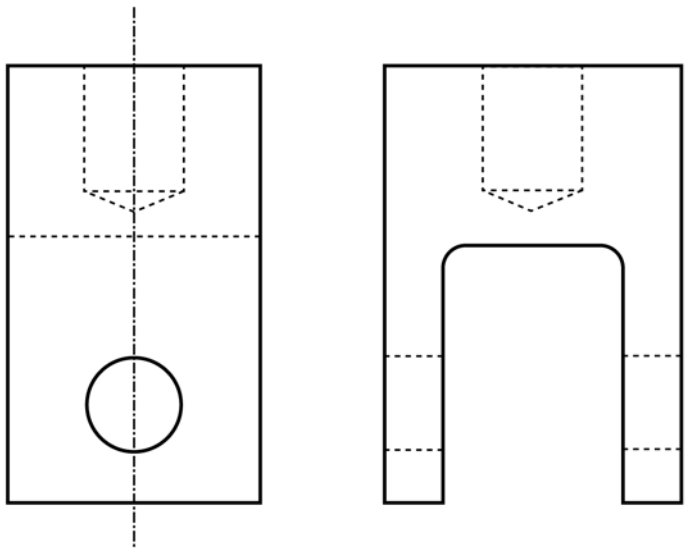

FIG. 3 Recommended Configuration of Tension Testing Clevis

NOTE 1—Flat bottomed holes are not required, but may be used in configurations found in Test Methods E399 or E1820.

3.2.2 *crack-mouth opening displacement, CMOD [L]*—see Terminology E1823 and Fig. 1 in this test method.

3.2.3 *force, P [F]*—see Terminology E1823.

3.2.4 *J-integral, J [FL^{-1} or FLL^{-2}]*—see Terminology E1823.

3.2.5 *modulus of elasticity, E [FL^{-2}]*—see Terminology E1823.

3.2.6 *net section area, A_N [L^2]*—see Terminology E1823. For surface cracks $A_N = WB - \pi a_0 c_0/2$.

3.2.7 *plane-strain fracture toughness, K_{Ic} [$FL^{-3/2}$]*—see Terminology E1823.

3.2.8 *Poisson's ratio,* ν—see Terminology E6.

3.2.9 *specimen thickness, B [L]*—see Terminology E1823 and Fig. 1 from this test method.

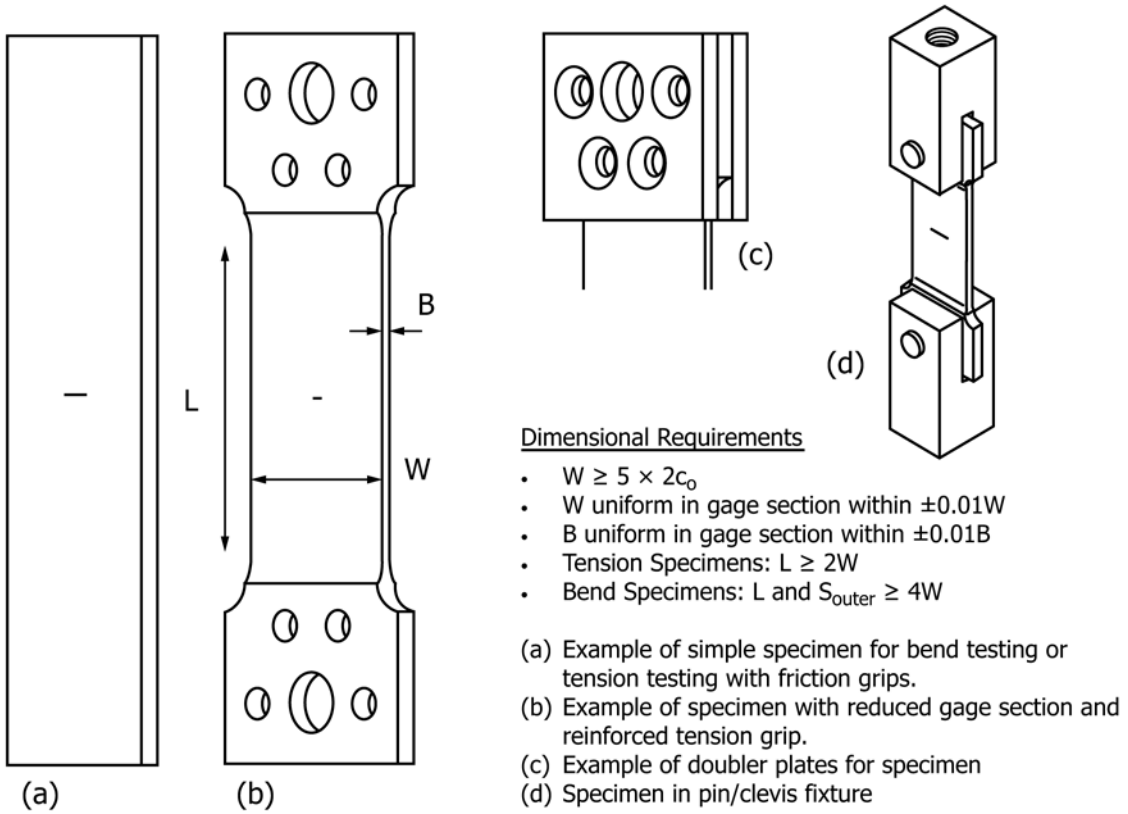

FIG. 4 Specimen Design Principles

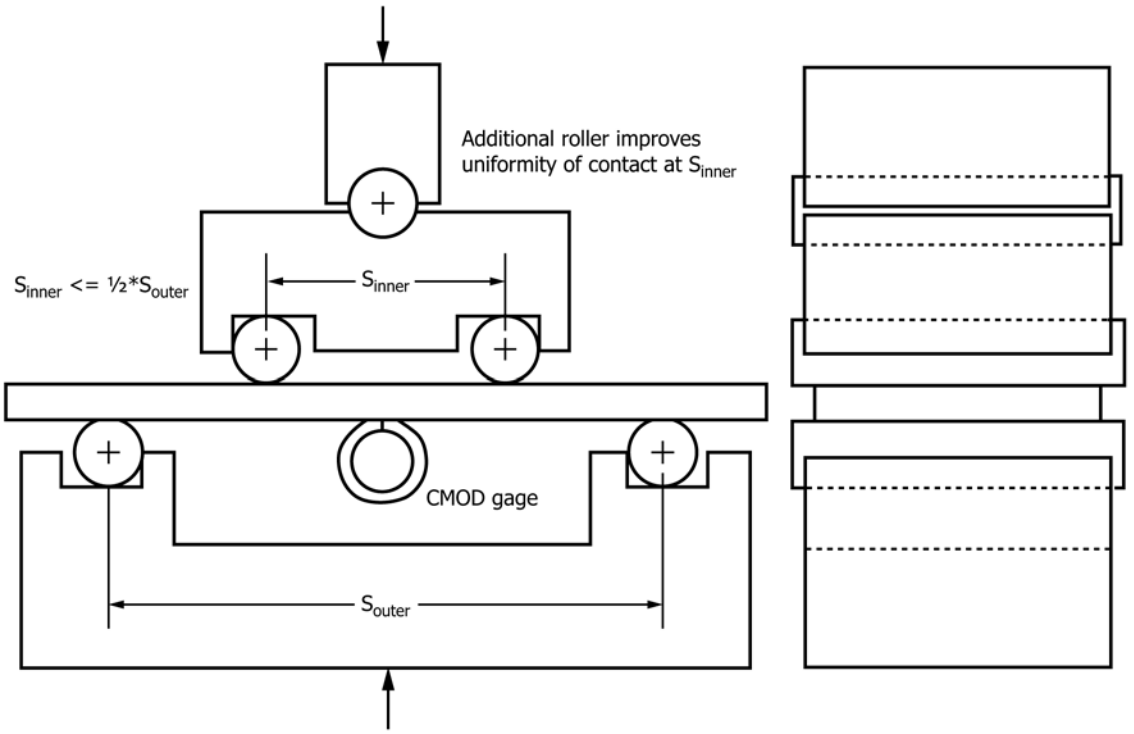

FIG. 5 Recommended Configuration of Bend Testing Apparatus

3.2.10 *specimen width, W [L]*—see Terminology E1823 and Fig. 1 from this test method.

3.2.11 *stable crack extension, [L]*—see Terminology E1823.

3.2.12 *stress ratio, R*—see Terminology E1823.

3.2.13 *surface crack length, 2c [L]*—see Terminology E1823 and Fig. 1 in this test method.

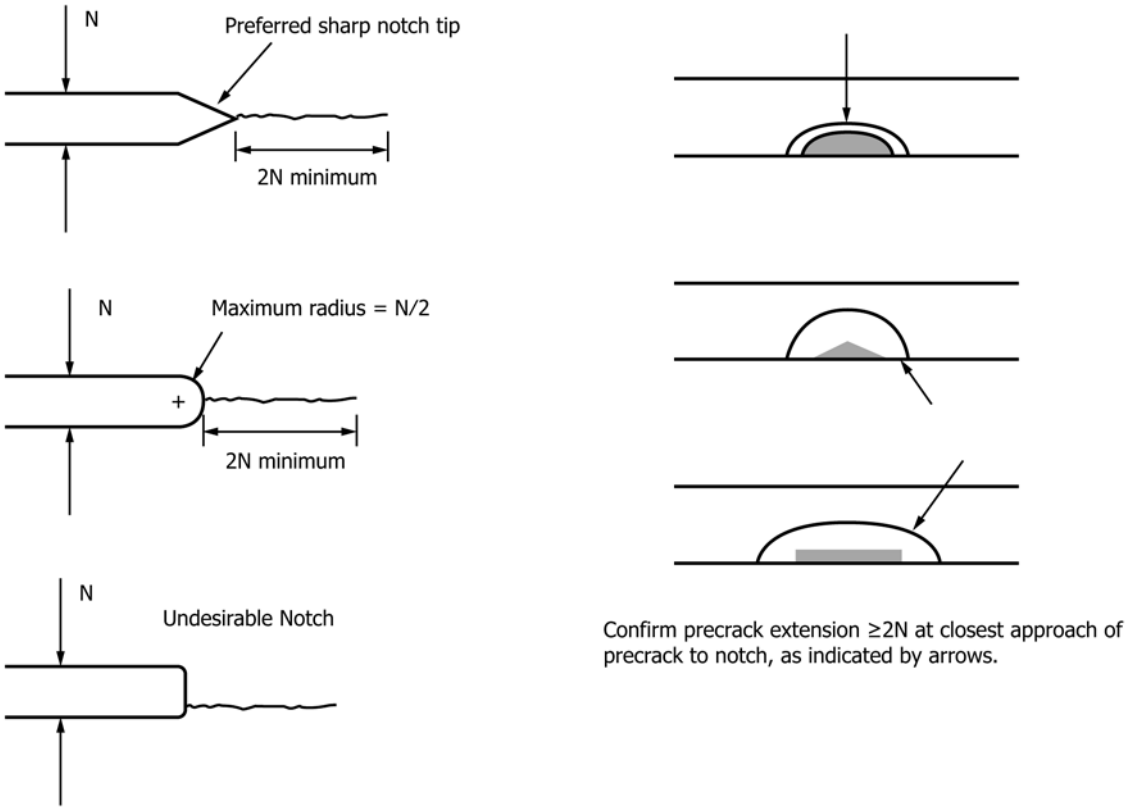

FIG. 6 Fatigue Crack Starter Notch Configuration

3.2.13.1 *Discussion*—In this test method, the term $2c_0$ is the original surface crack length, as determined in subsection 8.4, used in the evaluation of the test.

3.2.14 *yield strength,* σ_{YS} *[FL^{-2}]*—see Terminology E1823, as determined by 0.2% offset strain method.

3.3 *Definitions of Terms Specific to This Standard:*

3.3.1 *characteristic length,* $r_{\phi a}$, $r_{\phi b}$ *[L]*—a physical length measured post-test on the specimen fracture surface and compared to the length scale provided by the deformation limit. $r_{\phi a}$ is the distance measured on the crack plane normal to the crack front at the parametric angle ϕ_i to the front face (cracked face) of the specimen. $r_{\phi b}$ is the distance measured on the crack plane normal to the crack front at the parametric angle ϕ_i to the back face (uncracked face) or side of the specimen (Fig. A3.1).

3.3.2 *constraint,* Ω—in the context of this test method, constraint is a descriptor of the three dimensional stress and strain fields in the near vicinity of the crack tip where material contractions due to the Poisson effect may be suppressed and therefore produce an elevated, three-dimensional tensile (hydrostatic) stress state. An elevated hydrostatic stress state suppresses material yielding and permits larger stresses to develop. The material, geometry, and externally applied loads influence the development of the elevated hydrostatic stress state.

3.3.3 *elastic-plastic regime*—conditions in a test specimen where crack-tip deformations exceed limits of the linear-elastic regime defined in this test method, but J alone or J and a constraint term still characterize the crack-tip stress and strain fields. The non-dimensional parameters, C_{Ja} and C_{Jb}, define the deformation limits for validity of the elastic-plastic regime in this test method.

3.3.3.1 *Discussion*—Non-dimensional deformation limits such as C_K, C_{Ja} and C_{Jb} are commonly designated by the letter "M" in the literature (**5**).

3.3.4 *elastic-plastic regime crack size deformation limit,* C_{Ja}—the non-dimensional, upper limit of deformation for the elastic-plastic regime based on limiting the crack-tip opening displacement relative to the crack size.

3.3.5 *elastic-plastic regime ligament deformation limit,* C_{Jb}—the non-dimensional, upper limit of deformation for the elastic-plastic regime based on limiting plasticity in the remaining ligament.

3.3.6 *far field stress,* σ *[FL^{-2}]*—stress far removed from the crack plane resulting from applied forces or moments.

3.3.6.1 *Discussion*—For applied tensile forces, the far field stress is the average stress over the gross area, that is $\sigma = P/WB$. For applied bending moments, the far field stress is the maximum tensile outer fiber stress across the gross area, that is $\sigma = 6M/(WB^2)$.

3.3.7 *fatigue crack starter notch height, N [L]*—the height of the fatigue crack starter notch measured on the front face of the specimen prior to testing (Fig. 6).

3.3.8 *field-collapse regime*—conditions in a test specimen where crack-tip deformations exceed the limit of the elastic-plastic regime defined in this test method. Extensive plastic

deformation in the specimen eliminates the identifiable crack-front fields of fracture mechanics, which precludes analysis of test conditions in this test method.

3.3.9 *initiation angle,* ϕ_i—the parametric angle determined in accordance with Annex A5 that identifies the location along the crack perimeter where the test result is evaluated.

3.3.10 *initiation of surface crack extension*—in the context of this test method, the point during the test when, under monotonically increasing force or moment, the precrack extends a small but consistently measurable amount by stable, ductile tearing, or when the precrack extends in an immediate, unstable ductile mode, failing the specimen.

3.3.10.1 *Discussion*—Parameters associated with the initiation of surface crack extension are designated herein with a subscript *i* (for example, P_i) and define the state at which the crack front fields are characterized to render the toughness test result. The initiation of surface crack extension will generally be a local occurrence along the perimeter of a surface crack. Due to this localization, defining and experimentally quantifying a universal measure of relative or absolute crack extension for the surface crack geometry is not practical with commonly available laboratory equipment. Therefore, if identifiable, the extent and location of stable crack extension is recorded as an integral part of the test result. See subsection 8.3.4. In this context, the surface crack toughness result identifies a point on the material's tearing resistance curve as influenced by the local crack tip constraint conditions. See J-R curve and K-R curve definitions in Terminology E1823.

3.3.11 *initiation crack mouth opening displacement,* $CMOD_i$ *[L]*—the CMOD at which initiation of surface crack extension occurs.

3.3.12 *initiation force,* P_i *[F]*—the force at which initiation of surface crack extension occurs.

3.3.13 *initiation moment* M_i *[FL]*—the applied moment at which initiation of surface crack extension occurs.

3.3.14 *J-dominance*—crack-tip conditions where the elastic-plastic stress and strain fields are quantified by the value of the *J*-integral without constraint adjustment.

3.3.14.1 *Discussion*—Crack-tip fields described as *J*-dominant in this test method exist when elastic-plastic conditions develop at the crack front and high crack-tip constraint conditions prevail (for example, *T*-stress ≥ 0). *J*-dominant fields permit the use of a single parameter characterization of fracture toughness in terms of a critical *J*-value. In this test method, *J*-dominant conditions prevail to higher levels of crack-tip deformation than do *K*-dominant conditions.

3.3.15 J_K *[*FL^{-1} *or* FLL^{-2}*]*—a value of the *J*-integral calculated from K_I using the equation:

$$J_K = \frac{K_I^2\,(1 - \nu^2)}{E} \tag{1}$$

that is valid for linear-elastic, plane-strain conditions.

3.3.16 J_p *[*FL^{-1} *or* FLL^{-2}*]*—the peak value of the *J*-integral around the perimeter of the surface crack during monotonic loading.

3.3.17 J_ϕ *[*FL^{-1} *or* FLL^{-2}*]*—the *J*-integral value at the initiation angle (ϕ_i) when the specimen reaches the initiation crack mouth opening displacement ($CMOD_i$).

3.3.18 *K-dominance*—crack-tip conditions where the stress and strain fields immediately surrounding the crack-tip plastic zone are quantified by the stress intensity factor, K_I, without constraint adjustment.

3.3.18.1 *Discussion*—Crack-tip fields defined as *K*-dominant exist when globally linear-elastic conditions prevail in the specimen (see 3.3.23.1) together with high crack-tip constraint conditions (for example, *T*-stress ≥ 0). *K*-dominant fields permit the use of a single parameter fracture criterion expressed as a critical *K*-value, and are also *J*-dominant by definition.

3.3.19 K_p *[*$FL^{-3/2}$*]*—the peak value of the stress intensity factor around the perimeter of the surface crack during monotonic loading.

3.3.20 K_ϕ *[*$FL^{-3/2}$*]*—the stress intensity factor at the initiation angle (ϕ_i) with applied initiation force (P_i), or moment (M_i).

3.3.21 $K_{max\text{-}\phi}$ *[*$FL^{-3/2}$*]*—the maximum value of stress intensity occurring around the crack perimeter during fatigue precracking.

3.3.22 *length scale [L]*—a calculated length that is compared to a characteristic length ($r_{\phi a}$, $r_{\phi b}$) of the test specimen to evaluate the test result or determine test validity.

3.3.22.1 *Discussion*—The length scales are defined by a non-dimensional deformation limit, *C*, multiplied by the ratio of J/σ_{YS} in the form:

$$\text{length scale} = C\frac{J}{\sigma_{YS}} \tag{2}$$

3.3.23 *linear-elastic regime*—conditions in a test specimen where the stress and strain fields enclosing the crack-tip plastic zone are quantified by K_I alone, or by K_I and a constraint term.

3.3.23.1 *Discussion*—The linear-elastic regime applies when the amount of deformation at the crack tip remains small relative to the dimensions of the specimen. Conditions in the linear-elastic regime do not necessarily imply high constraint, for example, the *T*-stress may be positive or negative. The limit, C_K, sets the maximum deformation allowed at the crack tip for the linear-elastic regime in this test method.

3.3.24 *linear-elastic regime deformation limit,* C_K—the non-dimensional, upper limit of deformation for the linear-elastic regime.

3.3.25 *moment, M [FL]*—the value of the applied moment at the crack plane of a specimen during a test.
$M = (S_{outer} - S_{inner})\ P/4$ for four-point bending.

3.3.26 *normalized T-stress,* T/σ, T/σ_{YS}—*T*-stress divided by far-field stress or yield strength.

3.3.26.1 *Discussion*—T/σ is used as a first order measure of constraint, providing a definition and relative comparison of constraint for different crack geometries and loading conditions.

3.3.26.2 *Discussion*—T/σ_{YS} is used as a first order, quantifiable measure of constraint to describe crack front stress and strain fields.

3.3.27 *one-parameter fracture*—the use of K_I or J alone to describe fracture conditions when the crack-tip fields are K- or J-dominant as defined in this test method.

3.3.28 *parametric angle,* ϕ—the elliptic angle of position along the crack front, whereby the physical angle is transformed to a position on a semi-circle with radius a_o (Fig. 1).

3.3.29 Q—a non-dimensional parameter that describes the difference between the crack front stress field of interest relative to a common reference field.

3.3.29.1 *Discussion*—Q can be inferred by subtracting the crack front stress field for the $T = 0$ reference state from the stress field of interest in the specimen at a chosen normalized radial location in front of the crack tip on the crack plane. A commonly used definition of Q derives from a plane-strain, $T = 0$, reference field such that:

$$Q \equiv \frac{\sigma_{yy} - (\sigma_{yy})_{T=0}}{\sigma_0} \text{ at } \theta = 0 \text{ and } \frac{r\sigma_0}{J} = 2 \tag{3}$$

where σ_{yy} is the stress normal to the crack plane, r is the radial distance ahead of the crack tip on the crack plane (see Fig. 1), σ_0 is the flow stress (average of the yield and ultimate strength). Alternatively σ_{YS} can be substituted for σ_0 in the above equation.

3.3.30 Q_ϕ—value of Q at the initiation angle (ϕ_i) at deformation level corresponding to $CMOD_i$.

3.3.31 *inner span,* S_{inner}, L[L]—distance between inner specimen supports in the four-point bending configuration. See Fig. 5.

3.3.32 *outer span,* S_{outer}, L[L]—distance between outer specimen supports in the four-point bending configuration. See Fig. 5.

3.3.33 *specimen uniform cross section length,* L [L]—length of the center section of the specimen with uniform cross section. See Fig. 1.

3.3.34 *stress intensity factor,* K, K_J, K_I [$FL^{-3/2}$]—see Terminology E1823. All K-values in this test method refer to Mode I fracture.

3.3.35 *surface crack extension,* ℓ [L]—an increase in crack length measured normal to original crack front (Fig. 7). Differs from Terminology E1823 due to two-dimensional nature of the crack extension.

3.3.36 *two-parameter fracture*—the use of K_I or J together with a constraint term (such as T-stress or Q) to describe fracture conditions when the crack-tip fields are not K- or J-dominant.

3.3.37 *T-stress,* T [FL^{-2}]—a linear-elastic parameter used to quantify the first-order effects of constraint on near crack-tip stress and strain fields, and on the measured values of fracture toughness.

3.3.37.1 *Discussion*—T-stress is a scalar value appearing in the second term of the Williams power series expansion of the crack-tip stress fields, where the first two terms are given as:

$$\sigma_{ij}(r,\theta) = \frac{K_I}{\sqrt{2\pi r}} f_{ij}(\theta) + \begin{bmatrix} T & 0 & 0 \\ 0 & 0 & 0 \\ 0 & 0 & \nu T \end{bmatrix} \tag{4}$$

The νT term in σ_{zz} appears only for plane strain conditions. The T-stress term does not vary with r and θ.

3.3.37.2 *Discussion*—A specimen with geometry and loading combinations that create compressive (negative) T-stress has low crack front constraint (reduced hydrostatic stress) and, for most ductile fracture processes, may have a higher measured fracture toughness than specimens with a $T \geq 0$ configuration. A geometry and loading combination that creates tensile (positive) T-stress has high crack front constraint (increased hydrostatic stress) and may have a slightly decreased measured fracture toughness compared to the $T \leq 0$ configuration. See Appendix X4 for further discussion.

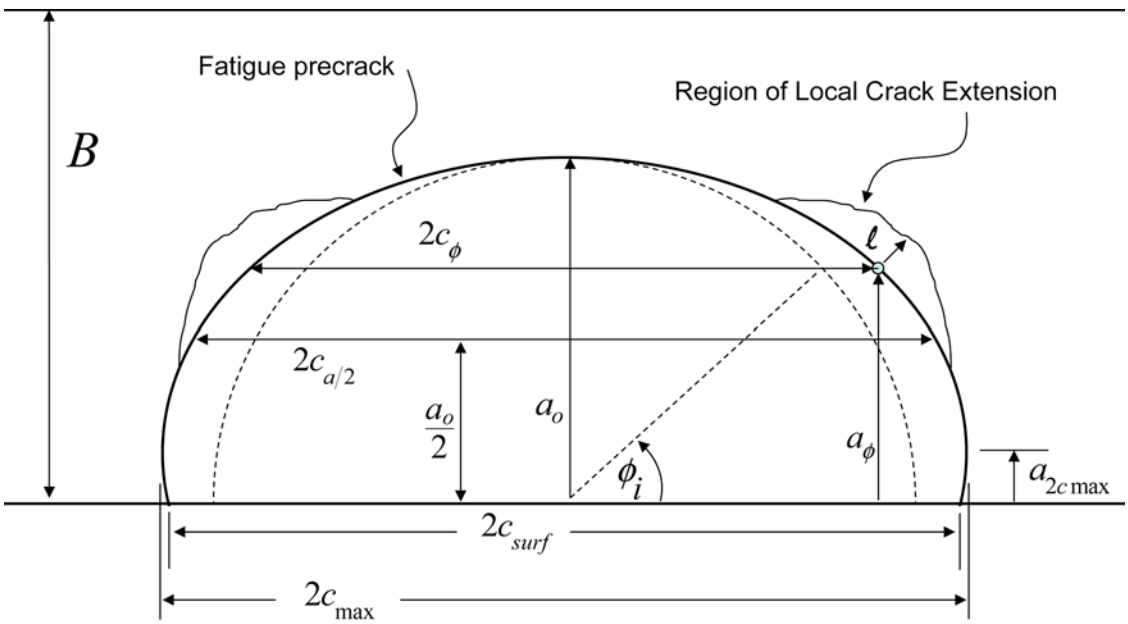

FIG. 7 Required Measurements of Precrack Dimensions and Crack Extension

3.3.37.3 *Discussion*—Some common negative *T*-stress configurations include SC(T), M(T), SE(B) with crack size to width ratio (*a/W*) of $a/W < 0.4$, and SE(T) with $a/W < 0.6$. Some common positive *T*-stress configurations include SC(B) with deep cracks, SE(B) with $a/W > 0.4$, SE(T) with $a/W > 0.7$, C(T), and DC(B).

3.3.38 T_ϕ *[FL^{-2}]*—*T*-stress at the initiation angle (ϕ_i) at deformation level corresponding to $CMOD_i$.

3.3.39 *unstable crack extension [L]*—an abrupt crack extension occurring with or without prior, stable crack extension.

4. Summary of Test Method

4.1 The objective of this test method is to obtain the fracture toughness of fatigue sharpened surface cracks in a constraint-based framework, where the toughness is measured either at the initiation of stable crack extension or immediate instability. The fracture toughness is quantified by either a single toughness value, or by two quantities, a toughness and a measure of constraint.

4.2 The test method consists of notching and fatigue sharpening (see Section 7) surface cracks into flat rectangular test specimens and then monotonically applying tension or bending force until the initiation of stable tearing is detected or immediate instability fails the specimen. The method requires at a minimum the continuous collection of force during the test. The continuous collection of CMOD is recommended for all tests, and is required when the limit of the linear-elastic regime is exceeded.

4.3 The method of detecting the onset of stable crack extension is not mandated by this test method; however, suggested methods are provided including electric potential drop, crack mouth opening displacement, acoustic emission, and replicate samples. Other methods are acceptable if validated as part of the test procedure.

4.4 The approach used to analyze the test results includes determining the location around the surface crack front where the initiation of crack extension occurred (ϕ_i). See Annex A5. Analysis of the test record then compares crack-front conditions and material properties against specific geometric length scales of the specimen to determine which regime appropriately describes the test conditions: linear-elastic regime, elastic-plastic regime, or the field-collapse regime.

4.5 If the test conditions do not lead to the field-collapse regime, the test result is classified into either the linear-elastic or the elastic-plastic regime. For tests demonstrating stable crack extension, the local length of surface crack extension is reported. If a one-parameter description of the crack tip fields is appropriate ($T_\phi \geq 0$) the result includes only K_ϕ or J_ϕ; otherwise, the result includes K_ϕ or J_ϕ along with the value of T_ϕ/σ_{YS} to complete a two-parameter description of the test.

5. Significance and Use

5.1 Surface cracks are among the most common defects found in structural components. An accurate characterization and understanding of crack-front behavior is necessary to ensure successful operation of a structure containing surface cracks. The testing of laboratory specimens with surface cracks provides a means to understand and quantify surface crack behavior, but the test results must be interpreted correctly to ensure transferability between the laboratory specimen and the structure.

5.2 Transferability refers to the capacity of a fracture mechanics methodology to correlate the crack-tip stress and strain fields of different cracked bodies. Traditionally, the correlation has been based on the presence at fracture of a dominant, asymptotically singular, crack-tip field with amplitude set by the value of a single parameter, such as the stress intensity factor, K_I, or the *J*-integral. For components and specimens with high crack-tip constraint, the singular crack-tip field dominates over microstructurally significant size scales for loads ranging from globally linear-elastic conditions to moderately large-scale plasticity. For specimens with low crack-tip constraint, a dominant single-parameter crack-tip field exists only at low levels of plasticity. At higher levels of plasticity, the opening mode stress of the low constraint specimen is lower than predicted by the single-parameter, asymptotically singular fields. Therefore, low constraint specimens often exhibit larger fracture toughness than do high constraint specimens. If feasible, users are strongly encouraged to generate high constraint fracture toughness data using methods such as Test Methods E399 or E1820 prior to testing the surface crack geometry.

5.2.1 To address this phenomenon, two-parameter fracture criteria are used to include the influence of crack-tip constraint. Crack-tip constraint has been quantified using various scalar parameters including the *T*-stress (**6**, **7**, **8**), *Q* (**9**, **10**), stress triaxiality (**11**, **12**), and α_h (**13**, **14**). Fracture toughness in a two-parameter methodology is not a single value, but rather is a curve that defines a critical locus of fracture toughness and constraint values (**2**). Fig. 2 illustrates a toughness-constraint locus for application of two-parameter fracture mechanics to structures. A structural analysis provides the driving force curve for the configuration of interest, and is plotted with the toughness-constraint locus obtained from specimen test data. Crack extension is predicted when the driving force curve passes through the toughness-constraint locus.

5.3 Tests conducted with this method provide data to assist in the prediction of structural capability in the presence of a surface crack by including a measure of crack-tip constraint in the interpretation of fracture toughness values. This improves the correlation of test specimen and structural conditions. To achieve the most accurate comparison, the conditions tested in accordance with this test method should match the structure as closely as possible. For conservative structural assessment, the user should ensure that conditions in the test specimen produce higher levels of constraint relative to the structure in application of the data. Factors that influence test specimen conditions include, but are not limited to, specimen geometry, *a/c*, *a/B*, loading conditions, as well as the amount and type of crack extension that occurred during the test.

NOTE 2—The use of a constraint-based framework for the analysis of surface cracks permits a more realistic assessment of structural capability. This approach generally leads to a less conservative assessment than would be achieved, for example, by using a measure of high-constraint fracture toughness obtained from testing standard C(T) and SE(B) specimens of the material following Test Method E1820. It is essential that

constraint effects measured in surface crack tests with this method be applied to any structural assessment with the requisite understanding to maintain appropriate levels of conservatism.

5.4 This test method does not address environmental effects or loading rate effects that may be significant in assessing service integrity.

6. Apparatus

6.1 Proper apparatus is required to meet the following minimum requirements: suitable test machine with proper measurement of applied force, instrumentation to record specimen displacements, and tension or bending clevises with associated fixturing. Additional apparatus may be useful to enhance the detection of surface crack extension. See subsection 6.4. The force and displacement measurements along with any supplemental instrumentation must be synchronized and fully recorded throughout the test, either digitally for processing by computer or autographically with an x-y plotter. The apparatus should be configured as mechanically stiff as possible to reduce stored elastic energy during the test. This significantly improves the ability to detect the initiation of stable crack extension.

6.2 *Force Measurement*—Testing machines shall have a force measurement capability conforming to the requirements of Practices E4. Applied force may be measured by any force transducer capable of being recorded continuously. Accuracy of force measurements shall be within 1% of the working range.

6.3 *Displacement Measurement*—A mechanical displacement gauge or other methods (for example digital image correlation) is used to measure the CMOD during the test to establish a force versus CMOD record. The CMOD measurement will aid in identifying the onset of stable tearing and enable verification of test assessment. CMOD measurement is required for all tests except those satisfying subsection 9.2.1, Linear-Elastic Regime Assessment, for which CMOD measurement and analytical confirmation are recommended, but not required.

6.3.1 All displacement gauges shall have a calibrated range no more than twice the maximum expected displacement during the test. The gauge accuracy shall be demonstrated to be within 1% of the full working range. Each gauge shall be verified for linearity using an extensometer calibrator or other suitable device. The resolution of the calibrator at each displacement interval shall be within 0.00051 mm (0.000020 in.). Readings shall be taken at ten equally spaced intervals over the working range of the gauge. The verification procedure shall be performed three times, removing and reinstalling the gauge in the calibration fixture after each run. The required linearity shall correspond to a maximum deviation of 0.003 mm (0.0001 in.) of the individual displacement readings from a least-squares-best-fit straight line through the data.

6.4 *Crack Extension Instrumentation*—This test method does not dictate the method(s) used to detect surface crack extension. Common methods include using the CMOD measurement, electric potential drop, or acoustic emission. Instrumentation shall be sufficiently calibrated to produce a consistent indication of surface crack extension and shall be recorded as stated in subsection 6.1 for archival use in evaluating the test results.

6.5 *System Verification*—It is recommended that the performance of the force and displacement measuring systems be verified before beginning a series of continuous tests. Calibration accuracy of displacement transducers shall be verified with due consideration for the temperature and environment of the test. Force calibrations shall be conducted periodically and documented in accordance with the latest revision of Practices E4.

6.6 *Fixtures:*

6.6.1 *Tension Fixtures*—The design of tension fixtures shall produce a uniform tension stress across the width and thickness of the specimen gauge section. Friction grips or pin and clevis arrangements are acceptable. Careful attention must be given to specimen and test machine alignment in either case. It is recommended, particularly with new specimen or clevis designs, that the uniformity of the tension stress be verified using a specimen instrumented with opposing strain gauges on an unnotched specimen. The uniformity of strain across all gauges should be confirmed as described in subsection 8.2.5.1. The clevis portion of a pinned specimen design is typical of those found in other fracture test standards. A common configuration is shown in Fig. 3. The flat bottomed holes required for clevises in other standards are not required for this method because specimen rotation is not a concern; clevis holes may be round. The clevis, pins and other fixturing must be fabricated from materials with sufficient strength to prevent yielding, brinelling, or excessive elastic deflection up to the maximum force encountered during test. Fixtures should be fabricated to high quality standards.

NOTE 3—Forces may be very high when testing tension specimens. Clevis designs must accommodate the stress and specimens using the pin and clevis design will often require reinforcement at the pin hole to prevent bearing yield or failure. This reinforcement can come from reducing the width, thickness, or both of the test section relative to the grip section or by adding supplemental doubler plates. See example specimen designs in Fig. 4.

6.6.2 *Bending Fixtures*—Fig. 5 shows the general proportions of acceptable four-point bend fixtures. The fixture design minimizes frictional effects by allowing the support rollers to rotate and move slightly apart as the force on the specimen increases, thus permitting rolling contact. The outer support rollers are allowed limited motion along plane surfaces parallel to the specimen, but are initially held against the inner stops with low tension springs (such as rubber bands).

7. Specimen Size, Configuration, and Preparation

7.1 *Principles of Test Specimen Design*—Basic features of surface crack specimen design are shown in Fig. 4. As discussed in Section 5, the intent of surface crack testing is commonly motivated by understanding the effects of surface cracks in structurally relevant configurations. In these situations, it is important that the test specimen represent the structure, primarily in thickness, crack size, and material condition. If the surface crack tests are not relevant to a specific structure, but are intended to characterize the general response of the material to surface defects, the specimen dimensions

should be established using the expected toughness and the length scales provided in subsections 9.2.1 (Linear-Elastic Regime Assessment) and 9.2.2 (Elastic-Plastic Regime Assessment), depending on which of these regimes is relevant to the designed test conditions. For general characterization, the crack configurations are recommended to span the range of $0.2 \le a/B \le 0.8$ and $0.1 \le a/c \le 1.0$. For practical purposes, the minimum crack dimensions permitted are: $a \ge 1.0$ mm and $c \ge 1.0$ mm (0.04 in.).

7.2 *Specimen Quantities*—The needed quantity of test specimens depends on the required reliability of the data. If the test results are to be used for design and evaluation of critical structures, sufficient tests to understand the variability of surface crack performance are strongly recommended. For general characterization, a minimum of three tests of a given specimen configuration is recommended. If multiple crack configurations are to be included in the test program, then replicates of each specimen are recommended.

7.3 *Tension Specimen Configuration*—Tensile test specimen proportions are shown in Fig. 4. The controlling proportions are $W \ge 5 \times 2c$ and $L \ge 2W$.

7.4 *Bending Specimen Configuration*—Bend test specimen proportions are shown in Fig. 4. The controlling proportions are $W \ge 5 \times 2c$ and $S_{outer}/W \ge 4$, where Fig. 5 defines the dimension S_{outer}.

7.5 *Specimen Precracking*—All specimens shall be precracked in fatigue. Experience has shown that it is impractical to obtain a reproducibly sharp, narrow machined notch that will simulate a natural crack well enough to provide a satisfactory fracture toughness test result. The most effective artifice for this purpose is a narrow notch from which extends a comparatively short fatigue crack, called the precrack. (A fatigue precrack is produced by cyclically loading the notched specimen for a number of cycles usually between about 10^4 and 10^6 depending on specimen size, notch preparation, and stress intensity level.) The dimensions of the notch and precrack, and the sharpness of the precrack shall meet specified conditions that can be readily met with most engineering materials.

7.5.1 *Surface Crack Precracking Objectives*—The precracking procedure must produce a fatigue crack of the intended length and depth with a regular semi-elliptical shape. The method of producing the starter notch and precrack should not influence the resulting fracture behavior of the test specimen. Fatigue loading may be applied through bending, tension, or a combination of both. The method of applying precrack forces may, and likely will, vary from that used for the actual monotonic test for surface crack extension. Precise control of the stress distribution across the specimen thickness during fatigue cycling is necessary to ensure the surface crack develops in the desired shape.

7.5.2 *Fatigue Crack Starter Notch*—Many different precrack starter notches are possible as shown in Fig. 6. The semi-elliptical starter notch is recommended to maximize the likelihood of producing a fatigue crack of proper shape with a minimum of fatigue crack growth, but other shapes may offer advantages or simplify to the notch machining. The starter notch may be cut by any available means. The plunge electrical discharge machining (EDM) method is the most common, but conventional machining techniques and laser cutting have been used effectively. The height of the notch, N, should be minimized. In practice, it should not exceed 1.0 mm (0.04 in.). As shown in Fig. 6, it is recommended that the notch end with a sharp "V" shape, and as a minimum the notch should end with a radius $\le N/2$. Generally, the effort to develop a technique for producing sharp notches is a good investment, because the time required to start the precrack is greatly reduced.

7.5.3 *Fatigue Precrack Shape and Length*—The fatigue precrack must be fully established around the full perimeter of the semi-ellipse. At all locations around the perimeter, the fatigue precrack shall extend a minimum $2N$ from the notch. The final shape shall be a semi-ellipse within the tolerance allowed in subsection 8.4. If additional features are machined into the starter notch for purposes of mechanical CMOD measurement, the precrack shall be sufficiently long to extend to or beyond a 60-degree envelope enclosing the starter notch and any features machined at the surface. See Fig. X3.1 for an illustration.

7.5.4 *Fatigue Precrack Procedures*—The following requirements shall be followed when producing the fatigue precrack.

7.5.4.1 *Fixtures*—The development of a regular semi-elliptical precrack is dependent on uniform stress distribution (tension or bending) over the specimen cross-section. Test fixtures and specimen alignment should be carefully addressed. The quality and precision of all precracking fixtures should be equivalent to those used for testing.

7.5.4.2 *Material Condition*—Fatigue precracking shall be performed with the material in the final heat-treated, mechanically worked, or environmentally conditioned state. Intermediate treatments between fatigue precracking and testing are acceptable only when such treatments are necessary to simulate the conditions of a specific structural application; such departure from recommended practice shall be explicitly reported.

7.5.4.3 *Fatigue Precrack Loading Requirements*—The maximum force applied to the specimen during precracking, including tension, bending, or combined tension/bending, shall limit the stress intensity to the lesser of $K_{max\phi} < 0.6K_{est}$ or $30MPa\sqrt{m}$ $(27ksi\sqrt{in})$ for the first 50% of the precrack and the lesser of $K_{max\text{-}\phi} < 0.5K_{est}$ or $25MPa\sqrt{m}$ $(22.8ksi\sqrt{in})$ for the final 50% of the precrack, where K_{est} is a provisional estimated material toughness and $K_{max\text{-}\phi}$ is the maximum value of stress intensity occurring around the crack perimeter as calculated by equations in Appendix X1. Precracking should be conducted at as low a $K_{max\text{-}\phi}$ as practical. $K_{max\text{-}\phi}$ is based on the instantaneous precrack size; therefore, forces required to achieve $K_{max\text{-}\phi}$ should be evaluated as the precrack grows. Small starting notches may result in high stresses to achieve the initial $K_{max\text{-}\phi}$ values allowed above. At no time during precracking shall the far field stress exceed 80% of the σ_{YS} (0.2% offset).

(1) Precracking forces are evaluated following the test by using K_ϕ in place of the provisional estimated toughness, K_{est}. To develop precracking parameters, K_{est} for the material may be estimated from the K_ϕ of previous surface crack tests or

from linear-elastic plane strain fracture toughness values determined by Test Method E399 or E1820. If no existing material toughness information is available, an acceptable limiting value of $K_{max\text{-}\phi}$ can often be estimated by ensuring $K_{max\text{-}\phi}/E < 0.00016\sqrt{m}$ $(0.001\sqrt{in})$, though not to exceed the values in subsection 7.5.4.3. This relationship may not sufficiently limit precracking conditions for high elastic modulus, low toughness materials such as very high strength steels.

(2) The stress ratio, R, during precracking is not prescribed, but is most commonly set at R = 0.1. Precracking may proceed as a single-step, multiple step, or continuous shedding process. If using the higher initial values of $K_{max\text{-}\phi}$ to hasten the initial 50% or less of precrack growth, then at least one additional step is required to complete the remaining 50% of the precrack with $K_{max\text{-}\phi}$ equal to or less than the values shown. Additional steps or automated load shedding may also be used to achieve this effect. An acceptable method for promoting fatigue crack initiation from the notch is to first apply compressive force cycles not exceeding the planned magnitude of the tensile fatigue precrack loads. If compressive forces are applied to tensile specimen designs (as opposed to bending), then buckling of the specimen must be avoided.

7.5.4.4 *Precracking and Test Temperature*—If the precrack and testing temperature are not the same, in addition to considering the potential for differing material toughness at the test temperature, the change in material strength must also be taken into account through the ratio of material yield strengths when estimating precracking stress intensity. Thus, this ratio is introduced into the relations of subsection 7.5.4.3 such that the stress intensity is limited to the lesser of

$$K_{\max-\phi} < 0.6\left(\sigma_{YS}^{precrack} / \sigma_{YS}^{test}\right) K_{est}$$

$$\text{or} \quad 30\ MPa\sqrt{m}\ \left(27_{ksi}\sqrt{in}\right)$$

for the first 50% of the precrack and the lesser of

$$K_{\max-\phi} < 0.5\left(\sigma_{YS}^{precrack} / \sigma_{YS}^{test}\right) K_{est}$$

$$\text{or} \quad 25\ MPa\sqrt{m}\left(22.8_{ksi}\sqrt{in}\right)$$

for the final 50% of the precrack, where $\sigma_{YS}^{precrack}$ is the 0.2% offset yield strength of the material at the precracking temperature and σ_{YS}^{test} is the 0.2% offset yield strength of the material at the test temperature. The limiting values $(30MPa\sqrt{m}$ and $25MPa\sqrt{m})$ remain unchanged. Environmental effects on material during precracking or test, other than temperature, are not within the scope of this test method.

8. Procedure

8.1 *Overview and Objectives*—The test procedure uses displacement control to apply monotonically increasing force or moment to a properly precracked test specimen until the crack begins to extend in a stable fashion, or until the specimen breaks due to unstable crack extension without any prior stable crack extension. If the specimen breaks due to unstable fracture without any prior stable crack extension, the initial crack size is measured and the location of the initiation of surface crack extension identified if possible. This information along with the applied force or moment is then used to evaluate the test in accordance with Section 9. If unstable fracture does not occur, the force and crack extension instrumentation are monitored continuously to detect the onset of stable crack extension. When stable crack extension is detected, the force or moment on the specimen is removed (or reduced) and a method of marking the current state of surface crack extension is applied to the test specimen. Finally, force or moment is re-applied in a monotonically increasing manner until specimen failure occurs. The initial crack size and crack extension are measured and are used along with the crack initiation force or moment to evaluate the specimen in accordance with Section 9.

8.2 *System and Test Preparation*—Prior to testing, all test apparatus shall be reviewed for compliance with the requirements and confirmed to be calibrated and fully functional.

8.2.1 *Pre-Test Measurement*—Record the following pretest specimen measurements to the nearest 0.025 mm [0.001 in.]: W, B, $2c_{surf}$, and N (precrack notch height at the surface). See Fig. 1, Fig. 6 and Fig. 7. The thickness B shall be an average of three measurements taken at the center and outside edges of the test specimen along the plane of the crack.

8.2.2 *Testing Rate*—All tests shall be conducted in displacement control. The rate of applied force or moment shall be quasi-static. A loading rate that produces stable crack extension or failure in 1 to 4 minutes is recommended, but shall not be less than 20 seconds. Data acquisition rates for electronic force and displacement measurements shall be commensurate to ensure a high fidelity test record. The time to reach the initiation of surface crack extension or failure shall be recorded for each test specimen. All specimens in a test series shall be loaded at the same nominal displacement rate.

8.2.3 *Test Environment*—The environment for conducting tests shall be carefully controlled and recorded as part of the test record.

8.2.4 *Temperature*—The temperature of the specimen shall be stable and uniform throughout the test within ± 3°C (± 5°F) and shall be recorded for each test. Temperature measurement capability must be accurate within ± 1°C (± 2°F). For other than ambient temperature tests, the specimen temperature shall be continuously monitored at a minimum of two locations within $W/4$ of the crack. Before testing in a liquid or gaseous medium for purposes of temperature control, the specimen shall be retained in the medium for at least 60 s/mm (150 s/0.1 in.) of thickness B after the specimen surface has reached the test temperature. Minimum soaking time at the test temperature shall be 15 minutes.

8.2.5 *Test Specimen and Fixture Alignment:*

8.2.5.1 *Overview*—The goal of mechanical alignment is to minimize unintended bending-induced non-uniformity in the stress applied to the specimen. The test frame and fixtures should apply a uniform uniaxial tension field or bending field across the width and through the thickness of the specimen. Each time the test system configuration is altered, the alignment of the test system should be confirmed using an unnotched specimen blank with strain gauges applied to verify uniformity within 10% of the strain field side-to-side (W-direction) and front-to-back (B-direction). Typical gauge placements for such purposes are illustrated in Practice E1012.

8.2.5.2 *Test Frame*—Test frame alignment is foundational to specimen and fixture alignment. Prior to evaluating fixture and

specimen alignment, verify test frame alignment based on the procedures in Practice E1012.

8.2.5.3 *Bend Testing*—Set up the bend test fixture so that the line of action of the applied force passes midway between the support roll centers within ±1% of the distance between the centers. Measure the spans to within ±0.5% of the nominal length. Locate the specimen so that the crack tip is midway between the rolls to within 1% of the span(s) and square to the roll axes. More so than with tension specimens, the front and back surfaces of the bend specimen need to be parallel planes, seating onto the rollers evenly across the specimen width. Confirmation of thickness uniformity in the vicinity of the roller contact lines is recommended.

8.2.5.4 *Tension Testing*—The centerline of the upper and lower loading rods or grip should be coincident within 0.25 mm (0.01 in.). Center the test specimen within the tension clevis or grips within 0.76 mm (0.03 in.).

8.3 *General Test Procedure:*

8.3.1 *Test Set-up*—Place specimen in test fixtures and attach all necessary instrumentation for monitoring temperature and identifying the onset of stable crack extension.

8.3.2 *Displacement Controlled Loading*—Properly zero tare values in instrumentation and then begin controlled ramp of test machine under actuator position control. Prepare to stop or reverse displacement whenever the instrumentation indicates stable crack extension has occurred. This may be an automated process if permitted by the instrumentation and data acquisition process.

8.3.3 *Unstable Crack Extension*—If the specimen breaks in an immediate fashion without stable crack extension, the test is completed. Measurements shall be taken in accordance with subsection 8.4, except surface crack extension (ℓ), and the test evaluated in accordance with Section 9.

NOTE 4—A material that fractures with a measureable J_{Ic} value in accordance with Test Method E1820, or that fractures with a Type I force versus displacement curve in a K_{Ic} test will experience stable crack extension in the surface-crack specimen configuration. If unstable crack extension cannot be avoided prior to detection of stable crack extension in these cases, the test apparatus is likely too compliant, thereby storing elastic energy and creating test conditions more similar to load control than displacement control. If the overall test apparatus can be stiffened, initiation of stable crack extension can likely be detected.

8.3.4 *Stable Crack Extension*—The force (P_i or M_i) and CMOD ($CMOD_i$) corresponding to the initiation of surface crack extension must be identified during the test. As discussed in 3.3.10.1, the localized nature of crack extension in the surface crack geometry precludes methods used to quantify crack extension in other fracture toughness test methods (for example, compliance). The user must develop a means to identify the point in the test when a consistently measureable amount of surface crack extension has occurred. The amount of surface crack extension identified as initiation is likely to vary from test to test. This variation requires the length of local surface crack extension (ℓ) to become an integral part of the test result, thus defining a location along the material's tearing resistance curve. Examples of techniques used to detect stable crack extension include the following:

(a) A particular characteristic feature in CMOD or acoustic emission results;

(b) Multiple replicate specimens for which each succeeding test is taken to a higher force (displacement), the force is reduced and the specimens are fatigue cycled to identify the extent and location of crack growth, and the specimens are then broken and examined;

(c) A specific change in electric potential measurements.

8.3.4.1 The recommended surface crack extension (ℓ) to be identified as initiation, measured locally on the perimeter normal to the crack front, is between 0.4 mm (0.016 in.) and 0.8 mm (0.032 in.). See Fig. 7. Using consistent amounts of crack extension from test to test is necessary if minimizing tearing resistance (*R*-curve) effects on the resulting measured toughness is important to the user. Further discussions regarding this section are found in Appendix X2 – Appendix X4.

8.3.4.2 *Marking of Stable Crack Extension*—If stable crack extension is detected, the amount of extension must be marked to permit post-test measurement. Once the initiation of surface crack extension has been indicated by instrumentation, and the force has been lowered or removed from the specimen, any number of methods may be used to mark the extent of stable tearing. The objective is to permit an accurate post-test measure of the precrack and the stable crack extension regions. A common method to mark the region of stable crack extension is to fatigue cycle the specimen at 60% of the maximum force with an *R*-ratio of 0.5 to 0.8. Other methods include heat tinting of steel and titanium alloys, staining of aluminum alloys with liquid sodium hydroxide, or fracturing susceptible steel alloys by cleavage at cold temperature. Any marking method using a liquid should be done with the specimen under moderate force to open the crack (typically ≤ 50% of P_i). In addition, the crack should be rinsed with a compatible volatile solvent and dried thoroughly to prevent bleeding into the fracture region when the specimen is broken. Liquid penetrants or inks which may remain wet in the crack are not recommended for marking surface crack extension.

8.3.4.3 *Failure After Stable Crack Extension*—After marking the region of stable crack extension, the specimen should be failed by monotonically increasing force or moment. The peak force or moment required to fail the specimen may be informative and is recommended to be recorded for possible use in residual strength assessments, with consideration that the failure load may be influenced by the method chosen to mark the surface crack extension.

(1) Discussion—For specimens which exhibit stable tearing, the final failure load represents the residual strength of the test specimen as the crack extension reaches the end of the stable region of the *R*-curve for that loading and geometry. This residual strength test result is utilized by Practice E740. In accordance with this test method, failure conditions following stable tearing shall not be characterized by K_I or J using the residual strength and the original (or fatigue marker band) crack length measurements. However, the residual strength information may have significance as an indicator of the slope and extent of the *R*-curve for the material, crack geometry, constraint conditions, given the compliance of the test system. The residual strength may also have particular relevance to

tests which are classified in the field-collapse regime (subsection 9.2.3). Application of residual-strength test data to structural applications requires additional considerations beyond the scope of this test method to ensure the test specimen appropriately represents the structure.

8.4 *Post-Test Crack Measurements and Evaluation*—After breaking the specimen, features of the fracture surface shall be measured carefully for use in the evaluations in accordance with Section 9. Measure the minimum distance of fatigue precrack extension from the notch, as shown in Fig. 6. Measure the following dimensions within ±0.05 mm (±0.002 in.): a_0, $2c_{surf}$, $2c_{a/2}$ (see Fig. 7). If $2c_{max}$ of the precrack does not occur at the surface, also measure the following: $2c_{max}$, $a_{2c\text{-}max}$. Determine ϕ_i in accordance with Annex A5, also recording the following dimensions within ±0.05 mm (±0.002 in.): a_ϕ, $2c_\phi$, ℓ. If unstable crack extension occurs as described in subsection 8.3.3, ℓ is not measured, but designated as "unstable crack extension." Calculate the values of $r_{\phi a}$ and $r_{\phi b}$ using the equations in Annex A3.

NOTE 5—A quality photograph with a precision scale in the view is strongly recommended for confirming measurements and providing a record of precrack shape and surface crack extension (ℓ) and location (ϕ_i).

8.4.1 *Precrack Length Evaluation*—At all locations (ϕ) around the fatigue precrack, the fatigue crack shall extend for a distance ≥ 2*N*, as measured normal to the local crack front, where *N* is the notch height measured at the surface pre-test. Only the shortest distance, as determined visually, must be confirmed by measurement.

8.4.2 *Precrack Shape Evaluation*—The precrack shall be evaluated for semi-elliptical shape.

8.4.2.1 If the maximum 2*c* dimension occurs at the surface, then $2c_0 \equiv 2c_{surf}$. Proceed to evaluations of $2c_\phi$ and $2c_{a/2}$ in accordance with 8.4.2.3.

8.4.2.2 If the maximum 2*c* dimension does not occur at the free surface, then evaluate the following two expressions: $2c_{max} \le 1.05 \times 2c_{surf}$ and $a_{2c\text{-}max} \le 0.1 \times a_0$. If both are true, set $2c_0 \equiv 2c_{max}$ and proceed to the evaluations of $2c_\phi$ and $2c_{a/2}$ in accordance with 8.4.2.3, otherwise the precrack is not sufficiently elliptical for evaluation in accordance with the analytical relations provided in this test method.

8.4.2.3 Calculate the values of $2c_{ellipse}$ at $a_0/2$ and a_ϕ by substituting these measured crack depths for $a_{measured}$ in Eq. 5. These values of $2c_{ellipse}$ must compare within ±5 % of their respective measured values, $2c_{a/2}$ and $2c_\phi$. If they do not, the precrack is not sufficiently elliptical for evaluation in accordance with the analytical relations provided in this test method.

$$2c_{ellipse} = 2c_0\sqrt{1 - \frac{a^2_{measured}}{a^2_0}} \tag{5}$$

8.4.3 *Precrack Force Evaluation*—Use K_ϕ from subsection 9.2.1.2 in place of K_{est} and verify requirements of subsection 7.5.4.3 or 7.5.4.4 as appropriate.

9. Analysis of Results

9.1 *Qualification of Data:*

9.1.1 All requirements on the apparatus in Section 6 shall be met.

9.1.2 All requirements in Section 7 pertaining to machining tolerances, specimen configuration, and precracking, including notch configuration, precrack length, and elliptical shape shall be met.

9.1.3 All requirements on fixture alignment, loading rate, test environment, and post-test precrack evaluations in Section 8 shall be followed.

9.2 *Determination of Deformation Regime*—The amount of deformation at the crack tip relative to the specimen size determines which of the three deformation regimes appropriately describes the test result: Linear-Elastic, Elastic-Plastic, or Field Collapse. Because constraint is characterized independently in the results analysis, the deformation regime is used only to determine the appropriate crack-front field parameter (*K*, *J*, or none), and not to ensure any specific level of specimen constraint. Fig. 8 illustrates the deformation regimes and example test loading paths which may end in any of five regions (A-E) based on the independent evaluation of deformation and constraint. Fig. 9 illustrates the how the non-dimensional deformation limits C_K, C_{Ja} and C_{Jb} define the three deformation regimes as a function of material elastic modulus to yield strength ratio.

9.2.1 *Linear-Elastic Regime Assessment:*

9.2.1.1 Use the initiation force (P_i) or moment (M_i) along with the specimen dimensions and crack dimensions to calculate the net section stress, $\sigma_{net}^{tension}$, for tension loading or σ_{net}^{bend} for loading in bending in accordance with equations provided in Annex A4. If $\sigma_{net}^{tension} > 0.9\sigma_{YS}$ for tension or if $\sigma_{net}^{bending} > 0.9\sigma_{YS}$ for bending, then assessment in the linear-elastic regime is not valid and the specimen shall be assessed for the elastic-plastic regime in accordance with subsection 9.2.2.

9.2.1.2 Calculate K_ϕ with the specimen dimensions, crack dimensions, initiation force (P_i) or moment (M_i), and the initiation angle (ϕ_i) using the equations in Annex A1.

9.2.1.3 Compute the quantities:

$$J_K = \frac{(K_\phi)^2(1 - \nu^2)}{E} \tag{6}$$

and

$$C_K = \frac{E}{\sigma_{YS}} \tag{7}$$

If $r_{\phi a}, r_{\phi b} \ge C_K(J_K/\sigma_{YS})$, and the net section stress requirements of subsection 9.2.1.1 are met, then assessment in the linear-elastic regime applies and K_ϕ is valid. See regions A and C in Fig. 8. If $r_{\phi a}, r_{\phi b} < C_K(J_K/\sigma_{YS})$, then assessment in the linear-elastic regime is not valid and the specimen shall be assessed for the elastic-plastic regime in accordance with subsection 9.2.2.

9.2.2 *Elastic-Plastic Regime Assessment:*

9.2.2.1 Calculate J_ϕ using specimen dimensions, crack dimensions, initiation force (P_i) or moment (M_i), the initiation CMOD ($CMOD_i$), and the initiation angle (ϕ_i). Calculation of J_ϕ must include the effects of plastic deformation. Finite element analysis in accordance with Annex A6 is required to compute the applicable value of J_ϕ.

(1) Accuracy of the analytically determined J_ϕ values shall be verified by comparison of force versus CMOD records from

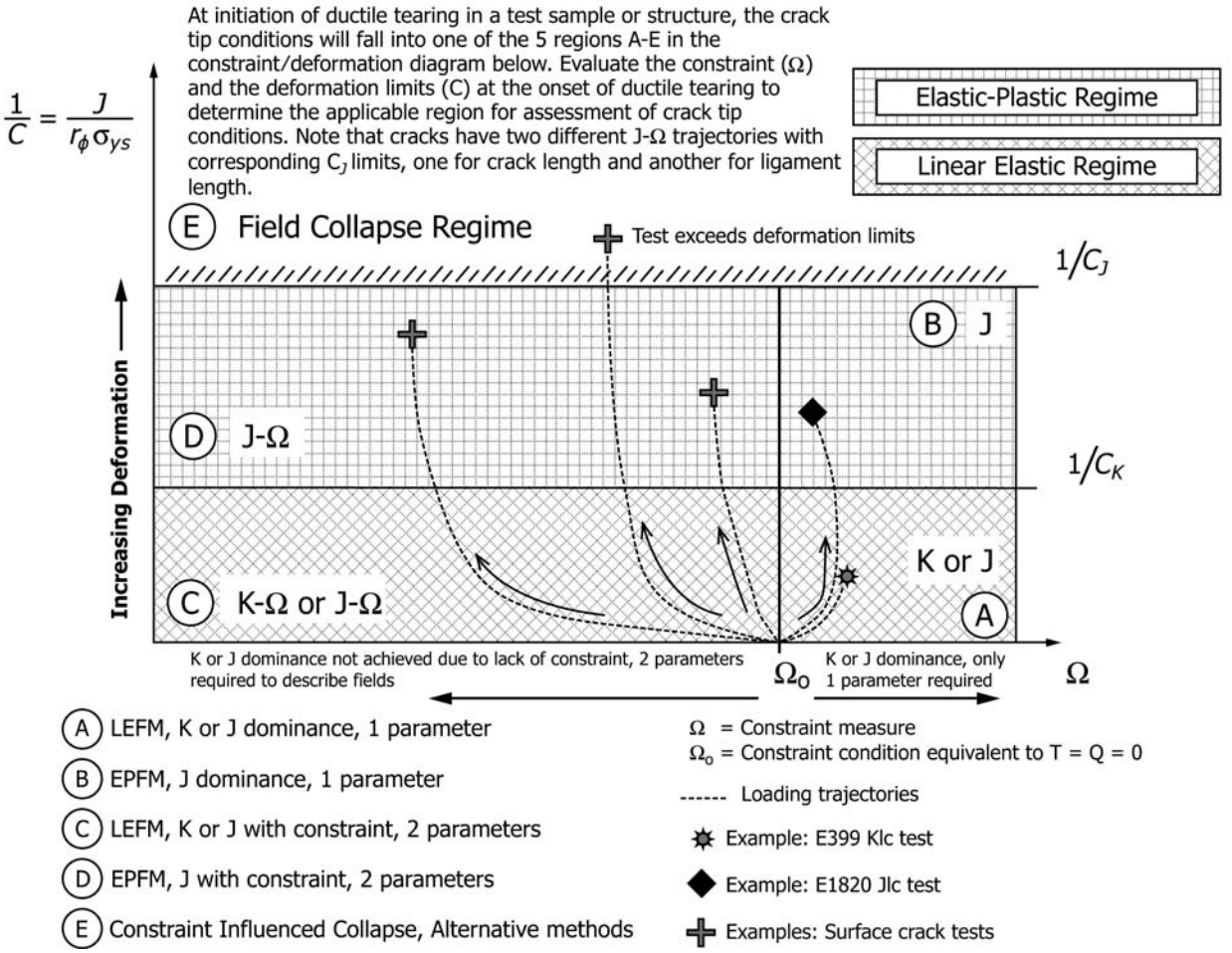

FIG. 8 Assessment of Crack Front Conditions

analysis and test. The requirements on analytically predicted force at $CMOD_i$ shall meet the requirements in Annex A6.

NOTE 6—In the elastic-plastic regime, J increases rapidly with continued loading. Agreement between analysis and measured force and displacement records provides requisite confidence in the computed J values.

9.2.2.2 Evaluate both specimen characteristic lengths, $r_{\phi a}$ and $r_{\phi b}$, against their respective elastic-plastic regime limits. Both evaluations must be true for valid use of the elastic-plastic regime.

(1) The amount of crack-tip opening displacement must be a small fraction of the crack size such that $r_{\phi a} \geq C_{Ja}(J_\phi / \sigma_{YS})$ where:

$$C_{Ja} = 15 \tag{8}$$

(2) The remaining ligament must have a sufficient size relative to the deformation such that $r_{\phi b} \geq C_{Jb}(J_\phi / \sigma_{YS})$ where:

$$C_{Jb} = \frac{1}{20}\frac{E}{\sigma_{YS}} + 50 \tag{9}$$

9.2.2.3 If $r_{\phi a} \geq C_{Ja}(J_\phi / \sigma_{YS})$ and $r_{\phi b} \geq C_{Jb}(J_\phi / \sigma_{YS})$ then assessment in the elastic-plastic regime applies and J_ϕ is valid (see regions B and D in Fig. 8). Otherwise, a transferrable J_ϕ value cannot be reported in accordance with this test method due to collapse of the crack-front strain and stress fields. In this case, assess the sample for field-collapse conditions in accordance with subsection 9.2.3.

NOTE 7—The deformation limit criteria of subsection 9.2.2 are set to sufficiently maintain crack front field integrity by limiting the influence of specimen boundaries on the fields. This provides a test result that is largely independent of specimen geometry and transferrable to other surface crack cases of similar constraint. In cases where the test specimens closely match the structural application in crack dimensions, specimen thickness, and net section stress, the concerns of transferability are minimized. For these cases, tests which exceed the deformation limits of subsection 9.2.2 may still provide useful evaluations of J and constraint relevant to the application. Tests at deformations exceeding the limits of subsection 9.2.2 should utilize direct measure of constraint, such as Q, rather than the elastic T-stress of subsection 9.3.

9.2.3 *Field-Collapse Regime Assessment:*

9.2.3.1 In the field-collapse regime, specimen deformations at the crack-tip exceed the limit of the elastic-plastic regime defined in this test method. Extensive plastic deformation in the specimen eliminates the identifiable crack-front fields of

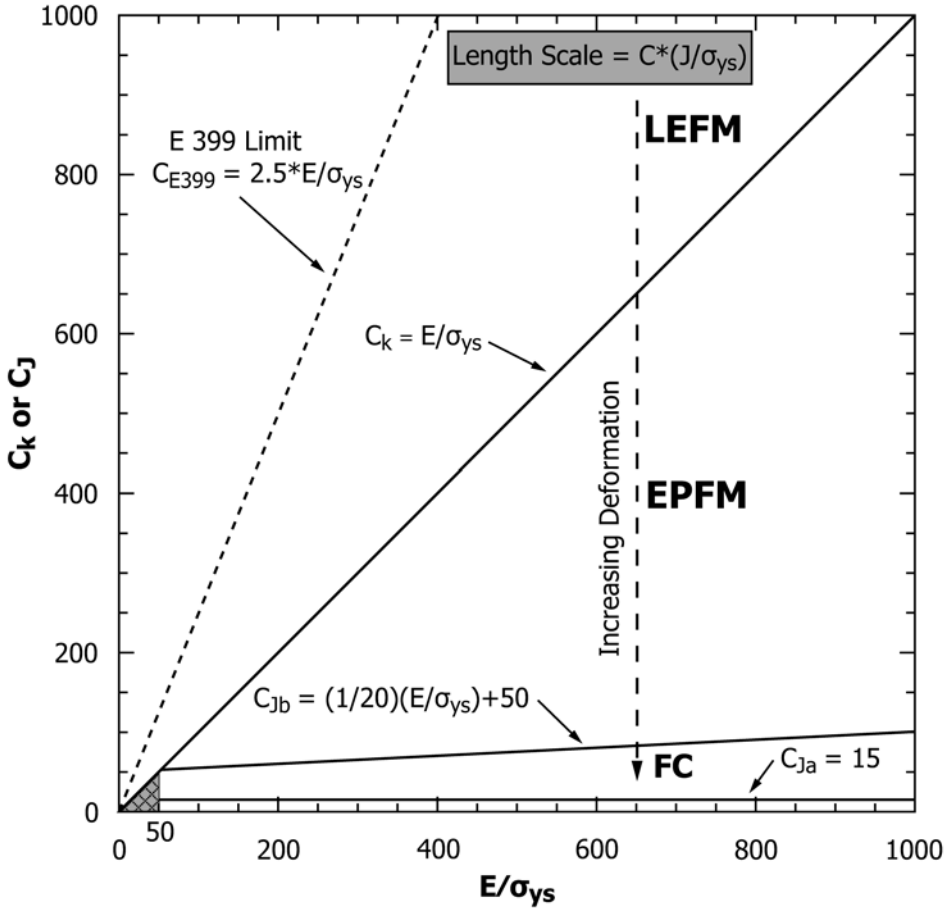

FIG. 9 Illustration of Crack Tip Deformation Increasing Through the Three Defined Regimes: Linear-Elastic Regime (LEFM), Elastic-Plastic Regime (EPFM), and Field Collapse Regime (FC), with Boundaries Defined by Nondimensional Deformation Limits C_K, C_{Ja}, and C_{Jb}.

fracture mechanics, which precludes analysis of test conditions in this test method. No K_ϕ or J_ϕ values shall be reported.

9.2.3.2 Assess specimens for crack-front field collapse conditions (see region E in Fig. 8) with failure assessment diagram (FAD) or other appropriate methods. Consider using methods: Fitness-for-Service API 579 (**15**), Guide on Methods for Assessing the Acceptability of Flaws in Metallic Structures, BS 7910:2005 (**16**). Alternatively conduct residual strength assessment of the specimen in accordance with Practice E740.

NOTE 8—Commercial services are available for elastic-plastic fracture mechanics analysis of surface crack test specimens. Consider organizations which provide fitness-for-service evaluations.

9.3 *Crack-front Constraint Assessment:*

9.3.1 This test method uses the elastic *T*-stress as a first order indicator of crack-front constraint and shall be recorded as part of the test result. Other measures of constraint may be used in a similar fashion and reported in addition to the *T*-stress, but it is the responsibility of the user to ensure the validity of the chosen constraint measure.

9.3.2 Calculate T_ϕ (*T*-stress at ϕ_i) using the tables in Annex A2.

9.3.3 If $T_\phi \geq 0$, then the crack-tip field is *K*-dominant for the linear-elastic regime or *J*-dominant for the elastic-plastic regime and may be described by K_ϕ or J_ϕ alone (one-parameter fracture). K_ϕ or J_ϕ values should be comparable to toughness values from testing deep notch SE(B) or C(T) specimens. See regions A and B in Fig. 8.

9.3.4 If $T_\phi < 0$, then the crack-tip field is not *K*-dominant or *J*-dominant, and two parameters are required to characterize the crack-tip field (two-parameter fracture). Characterize the crack-tip field condition by K_ϕ or J_ϕ and T_ϕ. See regions C and D in Fig. 8. Report T_ϕ normalized by the yield strength, T_ϕ/σ_{YS}. If this ratio is less than –1, report $T_\phi/\sigma_{YS} = -1$.

9.3.4.1 *Discussion*—Even though the *T*-stress provides a good, first-order indicator of constraint for elastic-plastic conditions, (**8, 17**), it remains a linear elastic concept; therefore, *T*-stress is only defined for the range $-1 \leq T/\sigma_{YS} \leq 1$.

9.3.4.2 *Recommended Practice*—To ensure surface-crack behavior for the tested material is transferable through constraint correction, compare K_ϕ or J_ϕ and T_ϕ/σ_{YS} to values obtained in specimens of variable constraint such as SE(B) with $0.1 \leq a/W \leq 0.3$ to create a toughness-constraint locus. See Fig. 2.

10. Report

10.1 The report should include the following for each specimen tested:

10.1.1 Specimen configuration and dimensions, including the crack starter notch dimensions and configuration;

10.1.2 Crack plane orientation;

10.1.3 Material designation (ASTM, AISI, SAE, and so forth) and material product form (plate, forging, casting, and so forth);

10.1.4 Yield strength (0.2% offset) and ultimate tensile strength measured in accordance with Test Methods E8/E8M;

10.1.5 If available, the results of high constraint fracture toughness tests from methods such as Test Methods E399 or E1820.

10.1.6 Maximum applied stress intensity factor during fatigue precracking, $K_{max\text{-}\phi}$, based on actual crack dimensions;

10.1.7 The number of fatigue cycles, the stress ratio (R), and their corresponding loading configuration: tension, bending, or combined tension and bending;

10.1.8 Fatigue crack depth, a_0, length, $2c_0$, and the results of the fatigue crack shape evaluation from subsection 8.4.2. A photograph of the fracture surface illustrating the fatigue precrack is recommended. Superimposing a semi-ellipse of depth a_0 and length $2c_0$ on the photograph is particularly helpful in evaluating the precrack shape and symmetry as well as measuring and documenting surface crack extension (ℓ) and location (ϕ_i);

10.1.9 Test temperature and environment. For tests at non-ambient conditions, include soak times prior to testing;

10.1.10 Determined value of initiation angle (ϕ_i) based on Annex A5;

10.1.11 The amount of stable, ductile surface crack extension (ℓ). For cases of unstable crack extension in accordance with subsection 8.3.3, designate ℓ as "unstable crack extension;"

10.1.12 The force P_i (or M_i) associated with initiation of surface crack extension;

10.1.13 The monotonic test time from the start of the force application to the point of initiation of surface crack extension or specimen fracture;

10.1.14 For tests in the elastic-plastic regime, the crack mouth opening displacement ($CMOD_i$) associated with initiation of surface crack extension;

10.1.15 Net section stress for tension or bending ($\sigma_{net}^{tension}$ or σ_{net}^{bend}) corresponding to P_i or M_i;

10.1.16 Specimen characteristic lengths, $r_{\phi a}$ and $r_{\phi b}$, at the location ϕ_i;

10.1.17 Length scale calculations in accordance with subsections 9.2.1 or 9.2.2 and comparisons with $r_{\phi a}$ and/or $r_{\phi b}$;

10.1.18 Test result classification as linear-elastic, elastic-plastic, or field-collapse regime;

10.1.19 Stress intensity factor for initiation of surface crack extension (K_ϕ) or J-integral value (J_ϕ). For test results in the field-collapse regime, K_ϕ and J_ϕ are not reported as fracture toughness values;

10.1.20 Test result classification as one-parameter or two-parameter fracture. If result is classified as two-parameter fracture, report T_ϕ/σ_{YS} at the location of ϕ_i;

10.1.21 Comparison of force (or moment) versus CMOD records from analysis and test when the test result lies in the elastic-plastic regime;

10.1.22 Any supplementary data used to help identify when stable crack extension occurred, such as a direct current potential drop signal.

11. Precision and Bias

11.1 *Precision*—The precision of any of the fracture toughness determinations cited in this test method is a function of the precision and bias of the various measurements of linear dimensions for the specimen and testing fixtures, the precision of the displacement measurement, the bias of the load measurement as well as the bias of the recording devices used to produce the load-displacement record, and the precision of the constructions made on this record. It is not possible to make meaningful statements concerning precision and bias for all these measurements. However it is possible to derive useful measurements concerning the precision of fracture toughness measurements in a global sense from inter-laboratory test programs, for example, (**18**).

11.2 *Bias*—There is no accepted standard value for any of the fracture toughness measures employed in this test method. Therefore, no meaningful statement can be made concerning bias of fracture toughness measurements.

12. Keywords

12.1 CMOD; constraint; crack initiation; crack mouth opening displacement; deformation limit; elastic-plastic regime; field-collapse regime; J-dominance; J-integral; K-dominance; length scale; linear-elastic regime; one-parameter fracture; stable crack extension; stress intensity factor; T-stress; two-parameter fracture; unstable crack extension

ANNEXES

(Mandatory Information)

A1. STRESS INTENSITY FACTOR EQUATIONS FOR SURFACE CRACKS IN A FLAT PLATE SUBJECTED TO TENSION AND BENDING

A1.1 This Annex provides equations to calculate the applied stress intensity factor (K_I) for flat specimens containing surface cracks. There is no exact solution for the problem of a semi-elliptical surface crack in a plate of finite dimensions. The following equations are taken from **(19)**, as modified later in **(20)**. The equations are curve fits to finite element calculations. These equations are considered to be sufficiently accurate for the purposes of this test method and are limited to cases where $a \le c$ and $a \le 0.8B$, where a is surface crack depth and c is half the surface crack length. Reference **(20)** extends the f_w term for tension to make it applicable for $W/2c \ge 1.25$

A1.2 For combined tension-bending loads, the stress-intensity factor equation is:

$$K_I = (\sigma_t F_t + H \sigma_b F_b)\left(\frac{\pi a}{Z}\right)^{1/2} \quad (A1.1)$$

with the following variables defined:

$$\sigma_t = \frac{P}{WB} \quad (A1.2)$$

$$\sigma_b = \frac{6M}{WB^2} \quad (A1.3)$$

$$Z = 1 + 1.464\left(\frac{a}{c}\right)^{1.65} \quad (A1.4)$$

$$F_t = \left[M_1 + M_2\left(\frac{a}{B}\right)^2 + M_3\left(\frac{a}{B}\right)^4\right] f_\phi f_{wt} g \quad (A1.5)$$

$$F_b = \left[M_1 + M_2\left(\frac{a}{B}\right)^2 + M_3\left(\frac{a}{B}\right)^4\right] f_\phi f_{wb} g \quad (A1.6)$$

$$M_1 = 1.13 - 0.09\left(\frac{a}{c}\right) \quad (A1.7)$$

$$M_2 = -0.54 + \frac{0.89}{0.2 + \frac{a}{c}} \quad (A1.8)$$

$$M_3 = 0.5 - \frac{1.0}{0.65 + \frac{a}{c}} + 14\left(1.0 - \frac{a}{c}\right)^{24} \quad (A1.9)$$

$$f_\phi = \left[\left(\frac{a}{c}\right)^2 \cos^2\phi + \sin^2\phi\right]^{1/4} \quad (A1.10)$$

$$f_{wt} = \left\{1 + \left[0.38\left(\frac{a}{c}\right)\left(\frac{a}{B}\right)\left(\frac{2c}{W}\right)^2 \cos\phi\right]\right\}\left\{\sec\left[\left(\frac{\pi c}{W}\right)\left[\left(\frac{a}{B}\right)(1 - 0.6\sin\phi)\right]^{1/2}\right]\right\}^{1/2} \quad (A1.11)$$

$$f_{wb} = \left\{\sec\left[\left(\frac{\pi c}{W}\right)\left(\frac{a}{B}\right)^{1/2}\right]\right\}^{1/2} \quad (A1.12)$$

$$g = 1 + \left[0.1 + 0.35\left(\frac{a}{B}\right)^2\right](1 - \sin\phi)^2 \quad (A1.13)$$

$$H = H_1 + (H_2 - H_1)(\sin\phi)^p \quad (A1.14)$$

$$p = 0.2 + \frac{a}{c} + 0.6\left(\frac{a}{B}\right) \quad (A1.15)$$

$$H_1 = 1 - 0.34\left(\frac{a}{B}\right) - 0.11\frac{a}{c}\left(\frac{a}{B}\right) \quad (A1.16)$$

$$H_2 = 1 + G_1\left(\frac{a}{B}\right) + G_2\left(\frac{a}{B}\right)^2 \quad (A1.17)$$

$$G_1 = -1.22 - 0.12\left(\frac{a}{c}\right) \quad (A1.18)$$

$$G_2 = 0.55 - 1.05\left(\frac{a}{c}\right)^{0.75} + 0.47\left(\frac{a}{c}\right)^{1.5} \quad (A1.19)$$

A1.3 Table A1.1 provides example values of stress intensity factors that may be used to verify implementation of these equations in computer programs or spreadsheets. Any consistent set of units for length and stress may be used.

TABLE A1.1 Validation Values of Stress Intensity (K_I) for Equations of Annex A1

Case	a	$2c$	W	B	σ_t	σ_b	ϕ (deg)	K_I
1	0.25	0.50	5.00	0.50	100.00	0.00	0	73.0
							30	64.3
							60	61.5
							90	61.3
2	0.25	0.50	5.00	0.50	100.00	50.00	0	101.3
							30	84.1
							60	74.2
							90	71.2
3	0.25	0.50	5.00	0.50	0.00	50.00	0	28.2
							30	19.8
							60	12.6
							90	9.9
4	0.40	4.50	5.00	0.50	100.00	0.00	0	232.8
							30	254.2
							60	263.0
							90	262.8
5	0.40	4.50	5.00	0.50	100.00	50.00	0	312.2
							30	321.1
							60	311.3
							90	302.3
6	0.40	4.50	5.00	0.50	0.00	50.00	0	79.4
							30	66.9
							60	48.2
							90	39.5

A2. NORMALIZED *T*-STRESS TABLES FOR SURFACE CRACKS IN TENSION AND BENDING

A2.1 This Annex provides tables to compute the *T*-stress for surface cracks in flat plates subjected to tension or bending. The values in the tables are from finite element analysis evaluations similar to those found in (**21**, **22**). Linear interpolation may be used to determine the *T*-stress value for specific combinations of *a/c*, *a/B* and ϕ that occur between the given table values.

A2.2 Flat Plate in Tension

A2.2.1 For Tables A2.1-A2.6, σ is the far field (gross) tensile stress on the specimen.

A2.3 Flat Plate in Bending

A2.3.1 For Tables A2.7-A2.12 σ is the far-field, maximum outer-fiber bending stress on the specimen based on properties of the gross cross-section.

TABLE A2.1 Normalized *T*-stress Values for Surface Crack in Tension with *a/c* = 0.1

Crack Front Angle, ϕ [deg]	Normalized *T*-stress (T/σ)				
	a/B = 0.1	*a/B* = 0.2	*a/B* = 0.4	*a/B* = 0.6	*a/B* = 0.8
5	-0.395	-0.404	-0.439	-0.489	-0.523
10	-0.471	-0.486	-0.532	-0.588	-0.614
15	-0.489	-0.500	-0.548	-0.576	-0.615
20	-0.496	-0.490	-0.547	-0.567	-0.568
25	-0.508	-0.498	-0.555	-0.576	-0.519
30	-0.519	-0.520	-0.566	-0.571	-0.480
35	-0.523	-0.528	-0.566	-0.557	-0.438
40	-0.524	-0.526	-0.566	-0.546	-0.394
45	-0.526	-0.526	-0.567	-0.535	-0.354
50	-0.528	-0.527	-0.568	-0.524	-0.316
55	-0.529	-0.528	-0.570	-0.513	-0.281
60	-0.530	-0.529	-0.571	-0.504	-0.251
65	-0.531	-0.531	-0.572	-0.494	-0.229
70	-0.532	-0.532	-0.574	-0.486	-0.215
75	-0.532	-0.532	-0.574	-0.479	-0.209
80	-0.532	-0.533	-0.575	-0.473	-0.208
85	-0.533	-0.534	-0.575	-0.470	-0.210
90	-0.533	-0.533	-0.575	-0.469	-0.213

TABLE A2.2 Normalized *T*-stress Values for Surface Crack in Tension with *a/c* = 0.2

Crack Front Angle, ϕ [deg]	Normalized *T*-stress (T/σ)				
	a/B = 0.1	*a/B* = 0.2	*a/B* = 0.4	*a/B* = 0.6	*a/B* = 0.8
5	-0.387	-0.386	-0.401	-0.410	-0.422
10	-0.402	-0.403	-0.416	-0.410	-0.352
15	-0.439	-0.440	-0.458	-0.442	-0.343
20	-0.464	-0.460	-0.482	-0.458	-0.331
25	-0.478	-0.471	-0.495	-0.463	-0.333
30	-0.489	-0.478	-0.504	-0.466	-0.347
35	-0.498	-0.488	-0.512	-0.470	-0.363
40	-0.505	-0.502	-0.520	-0.477	-0.384
45	-0.509	-0.511	-0.526	-0.486	-0.414
50	-0.511	-0.516	-0.531	-0.499	-0.448
55	-0.513	-0.516	-0.537	-0.513	-0.483
60	-0.514	-0.519	-0.543	-0.526	-0.517
65	-0.515	-0.520	-0.549	-0.539	-0.550
70	-0.516	-0.520	-0.554	-0.550	-0.581
75	-0.517	-0.522	-0.559	-0.559	-0.610
80	-0.517	-0.523	-0.562	-0.565	-0.633
85	-0.517	-0.523	-0.564	-0.569	-0.649
90	-0.517	-0.523	-0.565	-0.570	-0.656

TABLE A2.3 Normalized *T*-stress Values for Surface Crack in Tension with *a/c* = 0.4

Crack Front Angle, ϕ [deg]	Normalized *T*-stress (T/σ)				
	a/B = 0.1	*a/B* = 0.2	*a/B* = 0.4	*a/B* = 0.6	*a/B* = 0.8
5	-0.467	-0.518	-0.473	-0.497	-0.553
10	-0.423	-0.424	-0.417	-0.400	-0.366
15	-0.418	-0.418	-0.407	-0.369	-0.296
20	-0.428	-0.429	-0.414	-0.364	-0.268
25	-0.441	-0.442	-0.427	-0.369	-0.262
30	-0.454	-0.455	-0.441	-0.381	-0.281
35	-0.465	-0.464	-0.455	-0.397	-0.320
40	-0.474	-0.471	-0.467	-0.417	-0.371
45	-0.482	-0.476	-0.479	-0.441	-0.428
50	-0.489	-0.481	-0.491	-0.467	-0.491
55	-0.493	-0.486	-0.501	-0.494	-0.558
60	-0.497	-0.490	-0.511	-0.522	-0.624
65	-0.500	-0.494	-0.521	-0.548	-0.686
70	-0.502	-0.497	-0.529	-0.571	-0.741
75	-0.503	-0.500	-0.536	-0.591	-0.787
80	-0.504	-0.501	-0.541	-0.606	-0.822
85	-0.505	-0.502	-0.544	-0.615	-0.843
90	-0.505	-0.502	-0.545	-0.618	-0.853

TABLE A2.4 Normalized *T*-stress Values for Surface Crack in Tension with *a/c* = 0.6

Crack Front Angle, ϕ [deg]	Normalized *T*-stress (T/σ)				
	a/B = 0.1	*a/B* = 0.2	*a/B* = 0.4	*a/B* = 0.6	*a/B* = 0.8
5	-0.603	-0.590	-0.614	-0.615	-0.658
10	-0.495	-0.490	-0.496	-0.493	-0.495
15	-0.471	-0.466	-0.466	-0.449	-0.420
20	-0.464	-0.458	-0.456	-0.426	-0.380
25	-0.463	-0.456	-0.453	-0.416	-0.359
30	-0.467	-0.458	-0.456	-0.416	-0.358
35	-0.472	-0.462	-0.463	-0.423	-0.378
40	-0.477	-0.467	-0.471	-0.437	-0.415
45	-0.483	-0.472	-0.480	-0.455	-0.463
50	-0.489	-0.477	-0.490	-0.477	-0.522
55	-0.494	-0.483	-0.500	-0.502	-0.580
60	-0.499	-0.488	-0.509	-0.526	-0.641
65	-0.503	-0.493	-0.518	-0.550	-0.700
70	-0.506	-0.497	-0.526	-0.573	-0.755
75	-0.508	-0.500	-0.532	-0.592	-0.801
80	-0.510	-0.502	-0.537	-0.606	-0.836
85	-0.511	-0.503	-0.540	-0.615	-0.858
90	-0.511	-0.504	-0.541	-0.618	-0.868

TABLE A2.5 Normalized *T*-stress Values for Surface Crack in Tension with *a/c* = 0.8

Crack Front Angle, ϕ [deg]	Normalized *T*-stress (T/σ)				
	a/B = 0.1	*a/B* = 0.2	*a/B* = 0.4	*a/B* = 0.6	*a/B* = 0.8
5	-0.662	-0.646	-0.676	-0.718	-0.748
10	-0.561	-0.552	-0.568	-0.578	-0.590
15	-0.535	-0.527	-0.539	-0.535	-0.532
20	-0.523	-0.514	-0.524	-0.512	-0.501
25	-0.516	-0.505	-0.515	-0.497	-0.481
30	-0.512	-0.500	-0.510	-0.490	-0.472
35	-0.511	-0.498	-0.508	-0.488	-0.477
40	-0.511	-0.498	-0.509	-0.492	-0.495
45	-0.512	-0.499	-0.512	-0.501	-0.525
50	-0.514	-0.501	-0.517	-0.514	-0.562
55	-0.517	-0.505	-0.523	-0.529	-0.608
60	-0.520	-0.508	-0.529	-0.547	-0.655
65	-0.522	-0.512	-0.535	-0.565	-0.702
70	-0.524	-0.515	-0.540	-0.582	-0.748
75	-0.526	-0.517	-0.545	-0.597	-0.788
80	-0.527	-0.519	-0.549	-0.608	-0.819
85	-0.528	-0.520	-0.551	-0.616	-0.838
90	-0.528	-0.520	-0.552	-0.618	-0.847

TABLE A2.6 Normalized *T*-stress Values for Surface Crack in Tension with *a/c* = 1.0

Crack Front Angle, ϕ [deg]	Normalized *T*-stress (T/σ)				
	a/B = 0.1	*a/B* = 0.2	*a/B* = 0.4	*a/B* = 0.6	*a/B* = 0.8
5	-0.708	-0.690	-0.717	-0.761	-0.809
10	-0.615	-0.604	-0.622	-0.640	-0.669
15	-0.594	-0.583	-0.599	-0.607	-0.620
20	-0.583	-0.572	-0.587	-0.589	-0.596
25	-0.576	-0.563	-0.577	-0.576	-0.579
30	-0.570	-0.557	-0.570	-0.566	-0.572
35	-0.565	-0.552	-0.566	-0.561	-0.566
40	-0.562	-0.548	-0.563	-0.559	-0.575
45	-0.559	-0.545	-0.561	-0.560	-0.586
50	-0.557	-0.544	-0.560	-0.564	-0.612
55	-0.555	-0.543	-0.561	-0.571	-0.639
60	-0.554	-0.542	-0.562	-0.580	-0.675
65	-0.553	-0.542	-0.563	-0.590	-0.710
70	-0.552	-0.542	-0.565	-0.600	-0.743
75	-0.551	-0.542	-0.566	-0.610	-0.774
80	-0.551	-0.542	-0.568	-0.617	-0.795
85	-0.550	-0.542	-0.569	-0.622	-0.812
90	-0.550	-0.543	-0.569	-0.623	-0.813

TABLE A2.7 Normalized *T*-stress Values for Surface Crack in Bending with *a/c* = 0.1

Crack Front Angle, ϕ [deg]	Normalized *T*-stress (T/σ)				
	a/B = 0.1	*a/B* = 0.2	*a/B* = 0.4	*a/B* = 0.6	*a/B* = 0.8
5	-0.386	-0.385	-0.392	-0.400	-0.379
10	-0.444	-0.429	-0.407	-0.382	-0.315
15	-0.447	-0.413	-0.362	-0.306	-0.189
20	-0.439	-0.376	-0.306	-0.202	-0.052
25	-0.437	-0.356	-0.258	-0.105	0.056
30	-0.434	-0.350	-0.215	-0.034	0.171
35	-0.425	-0.332	-0.165	0.037	0.293
40	-0.415	-0.307	-0.118	0.116	0.414
45	-0.406	-0.286	-0.075	0.187	0.529
50	-0.397	-0.266	-0.036	0.257	0.642
55	-0.389	-0.249	-0.001	0.321	0.752
60	-0.382	-0.235	0.031	0.378	0.856
65	-0.376	-0.222	0.058	0.429	0.954
70	-0.371	-0.212	0.081	0.474	1.042
75	-0.367	-0.203	0.099	0.508	1.117
80	-0.364	-0.198	0.112	0.534	1.176
85	-0.362	-0.194	0.119	0.550	1.212
90	-0.362	-0.193	0.122	0.553	1.228

TABLE A2.8 Normalized *T*-stress Values for Surface Crack in Bending with *a/c* = 0.2

Crack Front Angle, ϕ [deg]	Normalized *T*-stress (T/σ)				
	a/B = 0.1	*a/B* = 0.2	*a/B* = 0.4	*a/B* = 0.6	*a/B* = 0.8
5	-0.382	-0.376	-0.377	-0.371	-0.354
10	-0.381	-0.361	-0.328	-0.280	-0.206
15	-0.402	-0.364	-0.303	-0.216	-0.088
20	-0.410	-0.354	-0.265	-0.142	0.033
25	-0.411	-0.336	-0.219	-0.063	0.140
30	-0.408	-0.316	-0.173	0.014	0.238
35	-0.403	-0.300	-0.129	0.087	0.331
40	-0.398	-0.288	-0.088	0.154	0.418
45	-0.390	-0.274	-0.048	0.215	0.498
50	-0.382	-0.258	-0.011	0.269	0.574
55	-0.375	-0.240	0.021	0.318	0.648
60	-0.368	-0.226	0.049	0.361	0.720
65	-0.362	-0.213	0.073	0.399	0.789
70	-0.357	-0.203	0.093	0.431	0.853
75	-0.353	-0.195	0.108	0.457	0.908
80	-0.350	-0.189	0.119	0.476	0.952
85	-0.348	-0.185	0.125	0.487	0.980
90	-0.348	-0.184	0.128	0.491	0.990

TABLE A2.9 Normalized *T*-stress Values for Surface Crack in Bending with *a/c* = 0.4

Crack Front Angle, ϕ [deg]	Normalized *T*-stress (T/σ)				
	a/B = 0.1	*a/B* = 0.2	*a/B* = 0.4	*a/B* = 0.6	*a/B* = 0.8
5	-0.464	-0.510	-0.460	-0.469	-0.489
10	-0.407	-0.392	-0.355	-0.312	-0.269
15	-0.388	-0.357	-0.286	-0.202	-0.108
20	-0.382	-0.337	-0.234	-0.111	0.028
25	-0.380	-0.320	-0.187	-0.030	0.147
30	-0.378	-0.305	-0.143	0.045	0.248
35	-0.376	-0.285	-0.100	0.114	0.336
40	-0.372	-0.268	-0.061	0.175	0.411
45	-0.368	-0.248	-0.024	0.230	0.482
50	-0.364	-0.233	0.010	0.279	0.543
55	-0.358	-0.218	0.040	0.319	0.598
60	-0.354	-0.206	0.066	0.354	0.648
65	-0.349	-0.194	0.088	0.383	0.697
70	-0.345	-0.185	0.106	0.407	0.742
75	-0.342	-0.178	0.120	0.425	0.782
80	-0.339	-0.172	0.129	0.439	0.814
85	-0.338	-0.169	0.135	0.447	0.834
90	-0.337	-0.168	0.137	0.449	0.842

TABLE A2.10 Normalized *T*-stress Values for Surface Crack in Bending with *a/c* = 0.6

Crack Front Angle, ϕ [deg]	Normalized *T*-stress (T/σ)				
	a/B = 0.1	*a/B* = 0.2	*a/B* = 0.4	*a/B* = 0.6	*a/B* = 0.8
5	-0.597	-0.579	-0.586	-0.567	-0.568
10	-0.478	-0.456	-0.427	-0.390	-0.358
15	-0.441	-0.405	-0.345	-0.272	-0.196
20	-0.419	-0.369	-0.278	-0.169	-0.056
25	-0.404	-0.339	-0.219	-0.077	0.075
30	-0.394	-0.313	-0.166	0.006	0.189
35	-0.385	-0.290	-0.117	0.081	0.287
40	-0.378	-0.270	-0.075	0.148	0.372
45	-0.371	-0.250	-0.034	0.207	0.447
50	-0.366	-0.235	0.001	0.258	0.510
55	-0.361	-0.220	0.032	0.302	0.569
60	-0.358	-0.208	0.059	0.338	0.618
65	-0.354	-0.197	0.082	0.370	0.662
70	-0.351	-0.189	0.101	0.393	0.702
75	-0.348	-0.182	0.115	0.412	0.736
80	-0.346	-0.176	0.126	0.425	0.762
85	-0.345	-0.173	0.132	0.432	0.780
90	-0.344	-0.172	0.134	0.435	0.786

TABLE A2.11 Normalized *T*-stress Values for Surface Crack in Bending with *a/c* = 0.8

Crack Front Angle, ϕ [deg]	Normalized *T*-stress (*T*/σ)				
	a/B = 0.1	*a/B* = 0.2	*a/B* = 0.4	*a/B* = 0.6	*a/B* = 0.8
5	-0.654	-0.631	-0.638	-0.647	-0.633
10	-0.541	-0.514	-0.488	-0.453	-0.416
15	-0.502	-0.462	-0.407	-0.336	-0.269
20	-0.476	-0.422	-0.337	-0.233	-0.129
25	-0.455	-0.386	-0.272	-0.138	-0.002
30	-0.438	-0.354	-0.214	-0.051	0.116
35	-0.423	-0.326	-0.160	0.030	0.222
40	-0.411	-0.301	-0.111	0.102	0.316
45	-0.401	-0.278	-0.066	0.167	0.399
50	-0.392	-0.260	-0.028	0.223	0.472
55	-0.385	-0.243	0.007	0.272	0.534
60	-0.379	-0.229	0.037	0.313	0.587
65	-0.374	-0.217	0.062	0.347	0.634
70	-0.370	-0.208	0.082	0.373	0.674
75	-0.367	-0.200	0.098	0.394	0.707
80	-0.364	-0.195	0.109	0.408	0.732
85	-0.363	-0.192	0.116	0.416	0.748
90	-0.363	-0.191	0.118	0.419	0.753

TABLE A2.12 Normalized *T*-stress Values for Surface Crack in Bending with *a/c* = 1.0

Crack Front Angle, ϕ [deg]	Normalized *T*-stress (*T*/σ)				
	a/B = 0.1	*a/B* = 0.2	*a/B* = 0.4	*a/B* = 0.6	*a/B* = 0.8
5	-0.698	-0.670	-0.672	-0.678	-0.690
10	-0.593	-0.562	-0.532	-0.498	-0.461
15	-0.558	-0.514	-0.455	-0.386	-0.321
20	-0.534	-0.475	-0.388	-0.288	-0.188
25	-0.512	-0.439	-0.324	-0.194	-0.059
30	-0.493	-0.406	-0.264	-0.106	0.052
35	-0.476	-0.376	-0.208	-0.024	0.168
40	-0.460	-0.348	-0.156	0.052	0.261
45	-0.446	-0.322	-0.109	0.121	0.355
50	-0.434	-0.300	-0.066	0.181	0.430
55	-0.422	-0.280	-0.028	0.235	0.497
60	-0.413	-0.263	0.005	0.281	0.557
65	-0.405	-0.248	0.032	0.318	0.603
70	-0.398	-0.236	0.055	0.348	0.646
75	-0.392	-0.227	0.073	0.371	0.679
80	-0.389	-0.220	0.086	0.387	0.704
85	-0.386	-0.216	0.093	0.397	0.720
90	-0.385	-0.215	0.096	0.400	0.725

A3. EQUATIONS FOR CALCULATION OF SPECIMEN CHARACTERISTIC LENGTHS

A3.1 This Annex provides equations to calculate the characteristic lengths, $r_{\phi a}$ and $r_{\phi b}$, for surface cracks. See Fig. A3.1. The characteristic lengths are compared to the length scales to determine the classification of a test result (see Section 9).

$$x_\phi = c_0 \times \cos(\phi) \tag{A3.1}$$

$$y_\phi = a_0 \times \sin(\phi) \tag{A3.2}$$

$$m = \frac{y_\phi c_0^2}{x_\phi a_0^2} \tag{A3.3}$$

$$x_{\text{int}} = x_\phi - \frac{a_0^2 \cos\phi}{c_0} \tag{A3.4}$$

$$x_e^{top} = x_\phi + \frac{B - y_\phi}{m} \tag{A3.5}$$

$$y_e^{side} = y_\phi + m(B - x_\phi) \tag{A3.6}$$

$$\text{If } x_e^{top} \geq \frac{W}{2} \rightarrow \begin{cases} x_e = \frac{W}{2} \\ y_e = y_e^{side} \end{cases} ; \quad \text{If } x_e^{top} < \frac{W}{2} \rightarrow \begin{cases} x_e = x_e^{top} \\ y_e = B \end{cases} \tag{A3.7}$$

$$r_{\phi a} = \sqrt{(x_\phi - x_{\text{int}})^2 + y_\phi^2} \tag{A3.8}$$

$$r_{\phi b} = \sqrt{(x_e - x_\phi)^2 + (y_e - y_\phi)^2} \tag{A3.9}$$

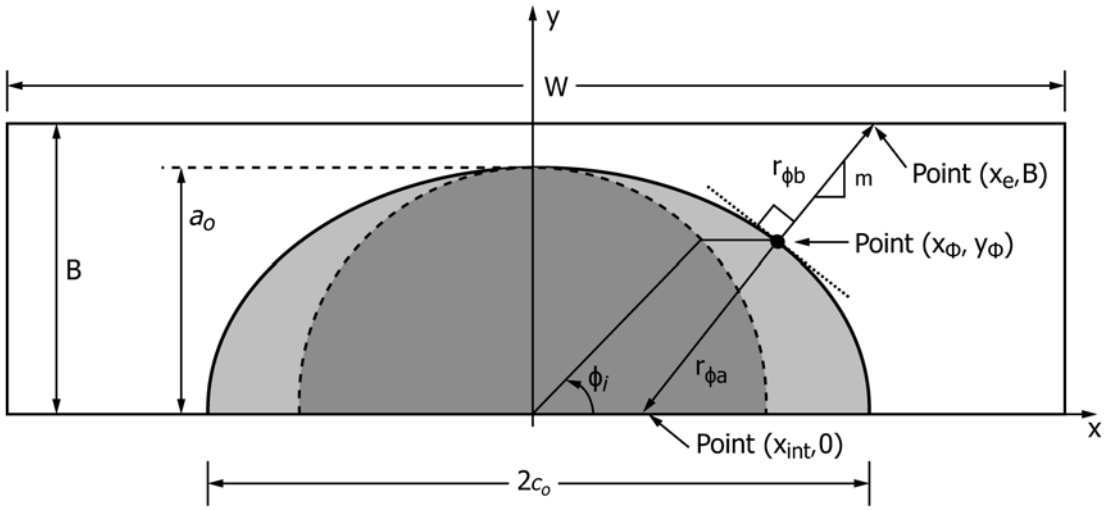

FIG. A3.1 Illustration of Variables for Characteristic Length Calculation

A4. EQUATIONS FOR ESTIMATION OF NET SECTION STRESS

A4.1 This Annex provides equations to estimate the net section stress near the crack for tension and bending loads for surface cracks. See Fig. A4.1. The net section stresses are compared to yield strength to assist in determining the applicability of the linear-elastic regime. The approximate position of the centroid of the net section is given by:

$$q_y = \frac{\frac{WB^2}{2} - \frac{2c_0a_0^2}{3}}{WB - \frac{\pi a_0 c_0}{2}} \tag{A4.1}$$

A4.1.1 The moment of inertia with respect to the centroidal coordinates is:

$$I_{\bar{x}} = \frac{WB^3}{12} + WB\left(q_y - \frac{B}{2}\right)^2 - \frac{\pi c_0 a_0^3}{8} - \frac{\pi c_0 a_0}{2}\left[\left(q_y - \frac{4a_0}{3\pi}\right)^2 - \left(\frac{4a_0}{3\pi}\right)^2\right] \tag{A4.2}$$

A4.1.2 From measured axial force, P_i and bending moment, M_i, the bending moment with respect to the centroidal coordinates, $M_{\bar{x}}$, is written as:

$$M_{\bar{x}} = P_i\left(q_y - \frac{B}{2}\right) + M_i \tag{A4.3}$$

A4.1.3 A moment that causes the crack mouth to open is defined as positive. The net section tension and bending stresses are then calculated as:

$$\sigma_{net}^{tension} = \frac{P}{WB - \frac{\pi a_0 c_0}{2}} \tag{A4.4}$$

and

$$\sigma_{net}^{bend} = \frac{M_{\bar{x}}}{I_{\bar{x}}}\left(q_y - \frac{a_0}{10}\right) \tag{A4.5}$$

A4.1.4 The bending stresses are calculated at points located a fraction (a_0/10) away from the outer boundary rather than exactly at the outer boundary based on the observation that plastic collapse does not occur as soon as the outer fibers reach yield strength.

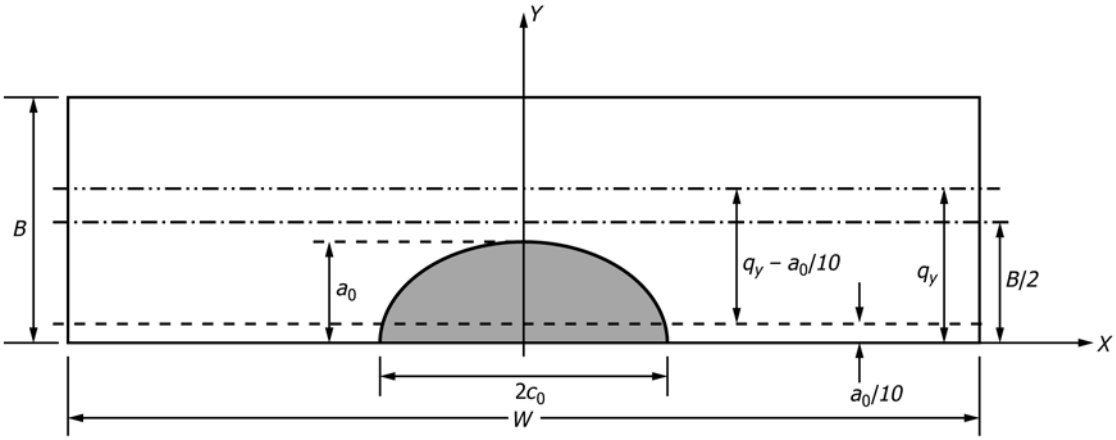

FIG. A4.1 Illustration of Variables for Net Section Stress Estimation

A5. METHODOLOGY FOR IDENTIFYING THE PARAMETRIC ANGLE ϕ_i CORRESPONDING TO THE POSITION OF MAXIMUM STABLE CRACK EXTENSION

A5.1 Determination of ϕ_i From Fracture Surface Evaluation

A5.1.1 Using a magnified image or photograph of the fracture surface, identify the location of maximum stable crack extension as measured normal to the elliptical precrack as shown in Fig. A5.1. The location along the precrack perimeter from which this normal vector emanates determines the value of ϕ_i. Measure the surface crack depth at this location, as indicated by a_ϕ in Fig. A5.1.

A5.1.2 If the surface crack extension is not symmetric around the precrack perimeter and the location of maximum surface crack extension occurs at $\phi_i > 90°$ utilize the mating fracture surface (or a mirror image) of the precrack such that $\phi_i \leq 90°$.

A5.1.3 Calculate ϕ_i using Eq A5.1. If $\phi_i < 5°$, set $\phi_i = 5°$.

$$\phi_i = \sin^{-1}(a_\phi \; / \; a_0) \tag{A5.1}$$

A5.1.3.1 *Discussion*—The 5° minimum value of ϕ_i accounts for the loss of crack-front singularity and the significant loss of constraint in material near the intersection of the crack front and the specimen surface. For most situations, crack-tip stress and strain fields are not sufficiently described by one- or two-parameter fracture this near a traction-free surface; therefore, this test method requires evaluation at least 5° away from the surface.

A5.2 Alternate Methodology for ϕ_i Estimation

A5.2.1 If ϕ_i cannot be identified from inspection of the fracture surface, estimate ϕ_i by finding the value of ϕ which maximizes $f(\phi)$ in Eq A5.2. If $\phi_i < 5°$, set $\phi_i = 5°$. The calculation of $J(\phi)$ and J_p shall include the effects of plastic deformation.

$$\begin{aligned} f(\phi) &= \frac{J(\phi)}{J_p}\left(\frac{T(\phi)}{\sigma_{YS}} + 1\right) \quad \text{for } \frac{T(\phi)}{\sigma_{YS}} \leq 0 \\ f(\phi) &= \frac{J(\phi)}{J_p}\left(\frac{T(\phi)}{4\sigma_{YS}} + 1\right) \quad \text{for } \frac{T(\phi)}{\sigma_{YS}} > 0 \end{aligned} \tag{A5.2}$$

The values for T/σ_{YS} as a function of ϕ are given in Annex A2. An example of graphically estimating ϕ_i from Eq A5.2 is shown in Fig. A5.2.

A5.2.2 A corresponding value of surface crack extension (ℓ) shall be specified along with the estimated ϕ_i from Eq A5.2. If the reason for using the A5.2 methodology is due to unstable crack extension preventing identification of ϕ_i from the fracture surface, the measure of surface crack extension (ℓ) shall be designated "unstable crack extension." However, if the need for A5.2 was due to measurable surface crack extension that was too uniform along the perimeter to distinguish ϕ_i, then the measure of surface crack extension (ℓ) shall be taken at the ϕ_i determined in A5.2.1.

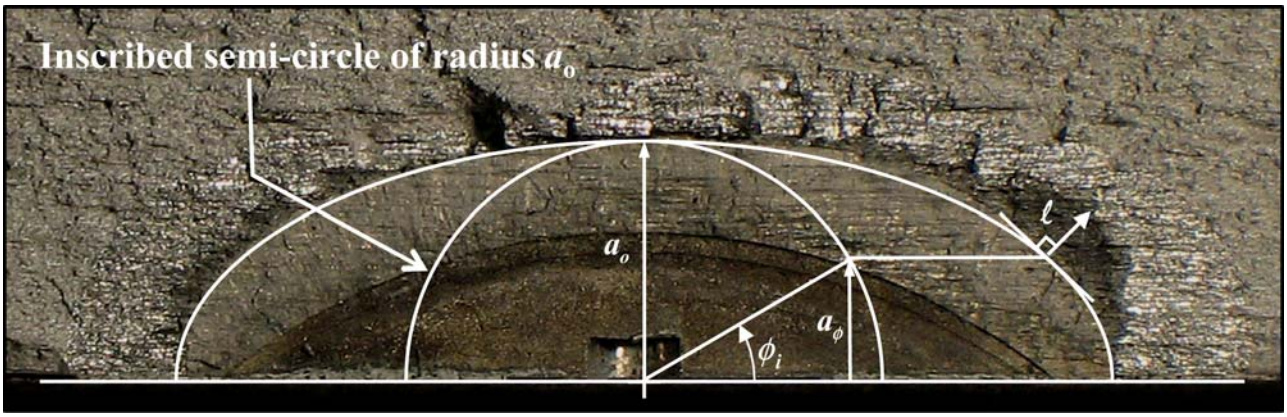

FIG. A5.1 Determination of ϕ_i from Specimen Fracture Surface..

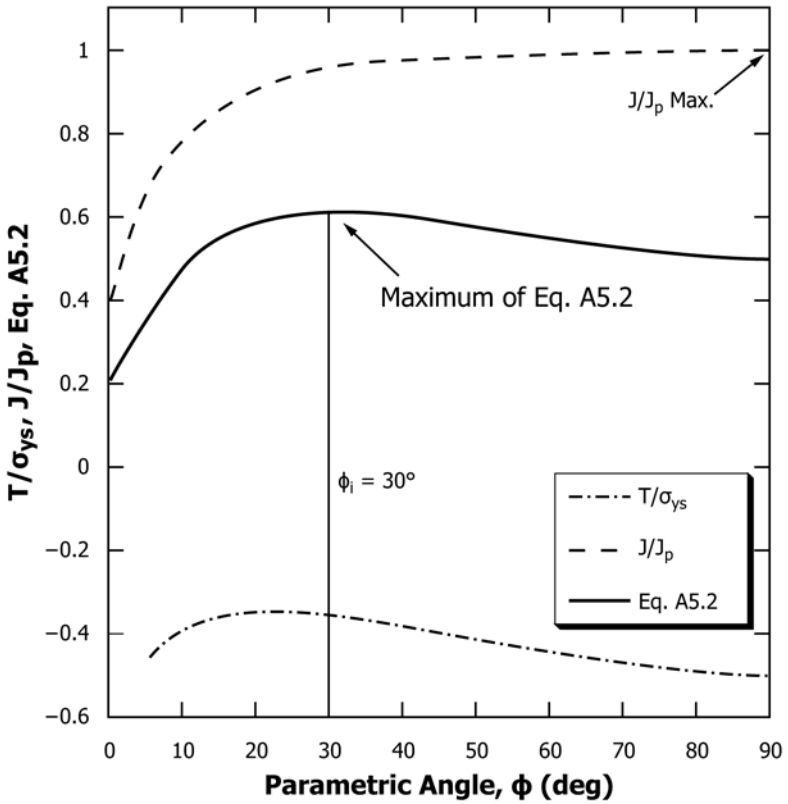

FIG. A5.2 Example of Determination of ϕ_i by Finding the Maximum of Eq A5.2.

A6. METHODOLOGY FOR PERFORMING ELASTIC-PLASTIC FINITE ELEMENT ANALYSIS AND COMPARISON TO TEST RECORD

A6.1 Introduction

A6.1.1 This Annex provides a methodology for performing elastic-plastic finite element analysis (FEA) of surface cracks in flat plates and the procedures for comparing the FEA values to the test record. The modeling requirements and recommendations in this annex were developed from the results of ASTM ILS 732 Analytical Round Robin for Elastic-Plastic Analysis of Surface Crack Plates. The results of ILS 732 are documented in (**23**).

A6.1.2 To maintain acceptable bounds on the analytical assessment of the experiment, the force-CMOD traces of the analysis and experiment should agree using reasonable metrics. Two assessments are used in this test method and are described in A6.3 and A6.4.

NOTE A6.1—For bending test evaluations substitute "moment" for "force" and M_i for P_i where appropriate.

A6.2 Methodology for Elastic-Plastic Finite Element Analysis

A6.2.1 In the development of a standardized test procedure, the objective is to provide all necessary controls to allow users to achieve a consistent test result. In the case of the elastic-plastic surface crack test, the approach used by other test standards, to contain all needed relations to evaluate the test record, is not currently feasible. The variations possible due to non-linear material behavior add sufficient complexity that an external, stand-alone analysis is required. ILS 732 has provided strong evidence that such a method is feasible without the introduction of excess variability, even without any significant guidance regarding the analysis methodology. However, ILS 732 has also provided clear insight into what common practices are in use, such that they could be standardized without undue burden on the user of the test method. This allows the test result to be standardized to the extent possible by providing specifics regarding what analysis practices are considered "standard." The following practices shall be followed for the elastic-plastic analysis of a surface crack test. As with any numerically estimated solution, it is recommended that the user confirm convergence of the finite element solution. Analyses meeting the prescribed practices in this Annex will provide sufficiently converged results for the *J*-integral.

A6.2.2 The analysis shall be performed using the finite element method.

A6.2.3 The model shall consist of 3-dimensional elements with quadratic shape functions and utilizing reduced integration. Full integration may be used for the first two rows of elements near the crack tip to avoid spurious zero energy deformation modes.

A6.2.4 The domain integral method shall be used for *J*-integral calculations.

A6.2.4.1 The domains should be as large as possible without compromising mesh integrity.

A6.2.4.2 The domains should consist of elements without excessive skew and should be normal to the local crack front within 30°.

A6.2.4.3 A minimum of five domains shall be used to monitor domain path dependence.

A6.2.4.4 All domain solutions shall be checked for path dependence, reporting only the highest converged value from the outer-most domain(s). Domain convergence is acceptable when the difference between the outer-most two domains is less than 2%. Unconverged domains indicate the physical size of the domain is too small for the deformation state in the model.

A6.2.4.5 All domain solutions shall be checked for oscillatory J-Integral results along the crack front. Solutions with node-to-node oscillations greater than 5% shall not be used.

A6.2.4.6 Small strain assumptions shall be used, such that the nodal geometry is not updated due to displacements.

A6.2.5 The following procedures shall be followed to develop constitutive model inputs:

A6.2.5.1 Tensile test data from Test Methods E8/E8M or equivalent is required to establish the stress-strain curve. The stress-strain curve shall be generated with continuous collection of strain data out to the ultimate strength of the material. Tensile specimens should come from the same material and metallurgical orientation used for surface crack testing. Multiple tests are preferable to evaluate a typical response.

A6.2.5.2 The finite element constitutive model shall follow Mises plasticity (incremental plasticity).

A6.2.5.3 Stress strain data shall be input as an incremental table of stress and strain values in the format required by the specific FEA code.

A6.2.5.4 Elastic modulus values shall come from either handbook values or dedicated modulus testing in accordance with Test Method E111 or equivalent.

(1) Discussion—Estimating elastic modulus from tensile tests is not recommended because the accuracy of the modulus measurement is strongly influenced by small amounts of bending during the test. True modulus of elasticity tests feature a balanced (or averaging) set of extensometry or strain gauges to account for the influence of bending. Note that modulus of elasticity is not a product of the tensile test in Test Methods E8/E8M.

A6.2.5.5 Use engineering stress-strain values to be compatible with the small strain assumption.

A6.2.5.6 Separate plastic strain from experimental stress-strain data by subtracting the elastic strain based on the best fit elastic modulus to the actual tensile test response (not the handbook value). If required, the quality of the linear fit should be biased toward the proportional limit region. Define the proportional limit at plastic strain consistently greater than 0.0001.

A6.2.5.7 Develop the input table as required by the analysis code (stress versus total strain or plastic strain). If the FEA code requires total strain input, then use the elastic modulus

value from A6.2.5.4 to calculate the elastic strain for a given stress value and sum the elastic and plastic strain components from A6.2.5.6 to calculate total strain. The table should have a sufficient number of entries to accurately define the proportional limit, roll-over, and tangent modulus characteristics of the stress-strain curve. The material model should be linear-elastic up to the proportional limit.

A6.3 Force-CMOD Elastic Compliance Comparison

A6.3.1 The elastic compliance of the force-CMOD relationship for the experiment and finite element model shall be compared. The compliance of most linear portion of the force-CMOD test record and the elastic compliance of the finite element analysis result shall match within ±5.0 %.

NOTE A6.2—Slight nonlinearity often occurs at the very beginning of a test record and should be ignored when calculating the elastic slope.

A6.3.2 This evaluation provides a broad check on numerous basic inputs to the analysis, including the specimen and crack geometry, the elastic stiffness in the material constitutive model, and to a lesser degree the modeled boundary conditions. Many fundamental analysis mistakes can be screened with this evaluation.

A6.3.3 Small changes in elastic modulus are permitted in the analysis to improve the elastic compliance match to the experiment; however, a need to alter the elastic modulus value in the analysis by more than ±5% to match the experiment is an indicator that some other aspect of the analysis or experimental data is incorrect. The modified elastic modulus value shall only be used in the finite element analysis to match the elastic compliance. All other instances of elastic modulus in this standard shall utilize the unmodified elastic modulus in accordance with 3.2.5 and A6.2.5.4.

A6.4 Force-CMOD Evaluation at Surface Crack Extension

A6.4.1 The force-CMOD response of the finite element model shall be compared to the test record P_i and $CMOD_i$ at surface crack extension.

A6.4.2 Determine the analysis reaction force corresponding to an analytical CMOD equal to $CMOD_i$ from the experiment. The analysis reaction force corresponding to $CMOD_i$ shall be within 5% of the experimental P_i. See Fig. A6.1.

A6.4.3 If the requirements of A6.3.1 and A6.4.2 are met, calculate J_ϕ corresponding to an analytical CMOD equal to $CMOD_i$ from the experiment. Otherwise J_ϕ cannot be reported from the analysis.

A6.4.4 The ±5% variation in analytical reaction force is allowed because test and analysis records seldom are an exact match. In general analyses behave stiffer than the experiment regarding the response to plastic deformation. This is an expected result from two perspectives. First, the finite element methodology discretizes the geometry and enforces an assumed displacement field within each of the elements, creating a model response stiffer than reality. Second, the nonlinearity in the experimental force-CMOD trace incorporates plasticity as well as geometric changes such as localized tearing; therefore, the test record nonlinearity may have plastic CMOD offset and elastic compliance changes due to surface crack

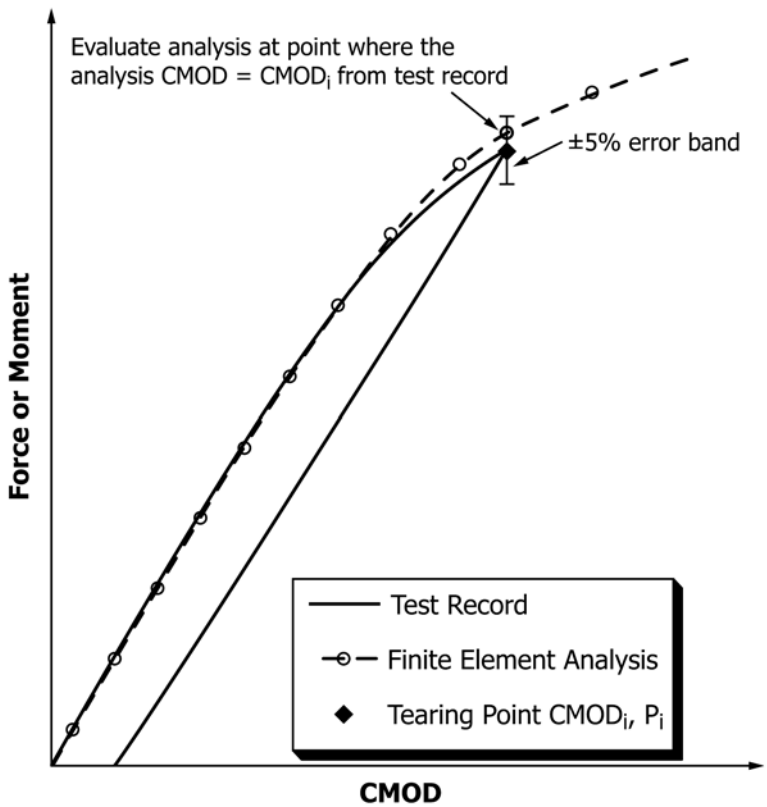

FIG. A6.1 Evaluate the Test Analysis by Matching CMOD Values

extension superimposed. The crack geometry in the analysis does not change—creating a stiffer analytical response. It is important that the test record not have excessive compliance change due to surface crack extension (tearing) in order for this assessment methodology to apply, that is, the crack shape after tearing should not be appreciably different from the precrack shape.

APPENDIXES

(Nonmandatory Information)

X1. PRECRACK SIZE AND SHAPE CONTROL

X1.1 *Overview*—The development of appropriately shaped, repeatable precracks is commonly the most time-intensive aspect to testing surface crack specimens. Time spent developing a repeatable methodology for this process is generally a good investment. There are two common approaches for producing a surface crack of a specified size. One allows the precrack shape to evolve by the fatigue process from an initial machined notch into the desired shape. The other attempts to curtail this natural shape evolution using a minimal amount of fatigue growth from an initial notch sized close to the target precrack dimensions.

X1.2 *Crack Shape Evolution*—Surface cracks in flat plates subjected to fatigue cycling in pure tension or bending tend to evolve toward a specific aspect ratio as a function of the depth to thickness ratio. Figs. X1.1 and X1.2 qualitatively illustrate the shape evolution for the tension and bending case, respectively. Understanding this behavior facilitates the production of target precrack sizes, especially for initial shapes which lie close to the preferred propagation path. Note that the preferred crack propagation path is slightly dependent on the fatigue crack growth exponent, n, as commonly expressed $da/dK = C(\Delta K)^n$, and assumes the entire crack front experiences ΔK well above the fatigue threshold. For $2 \le n \le 4$, the typical range of most common metals, the preferred propagation path for tension is approximated by (24):

$$\frac{a}{c} = 1 - 0.2\left(\frac{a}{B}\right)^2 \tag{X1.1}$$

and for bending by

$$\frac{a}{c} = 1 - \frac{a}{B} \tag{X1.2}$$

each valid for

$$\frac{a}{B} \le 0.7 \tag{X1.3}$$

X1.2.1 In tension, surface cracks will tend toward a semicircular shape, becoming slightly more elliptical as the crack depth approaches the back face of the specimen. In bending, cracks will tend toward a highly elliptical shape as the bending

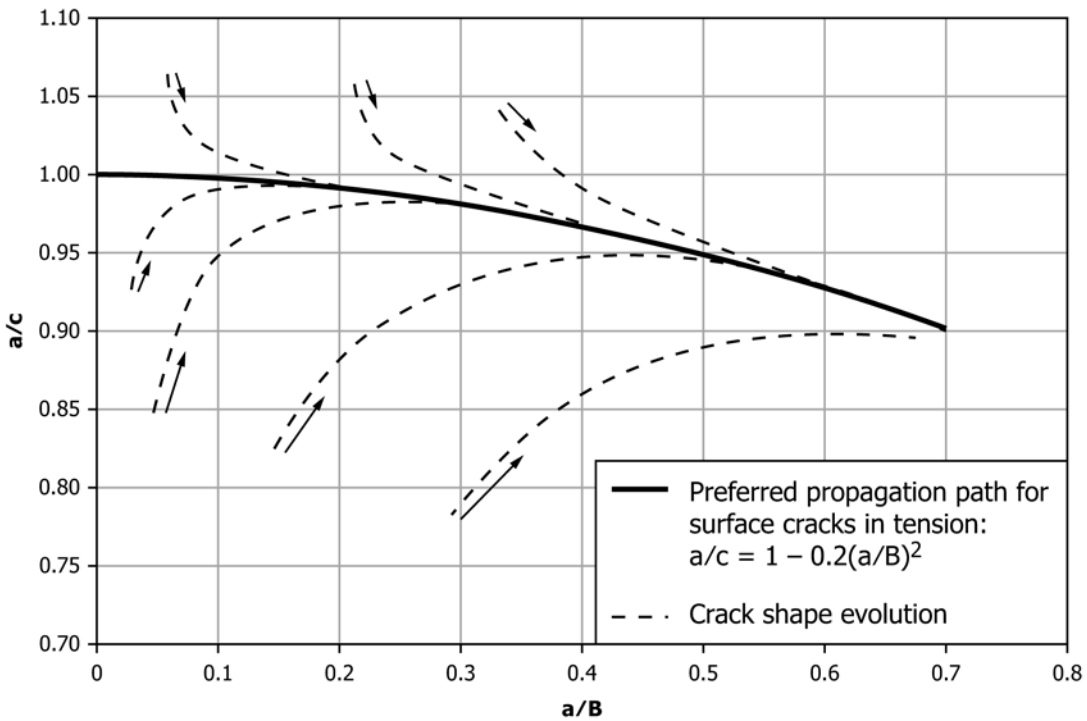

FIG. X1.1 Preferred propagation path of surface cracks in tension fatigue

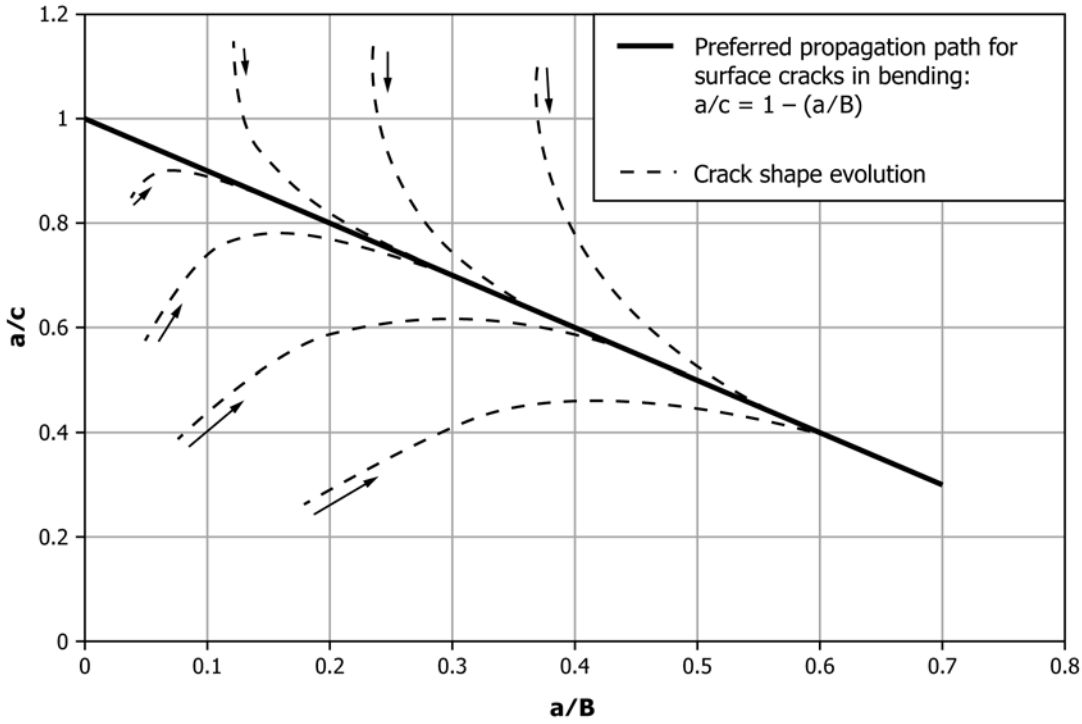

FIG. X1.2 Preferred propagation path of surface cracks in bending fatigue

stress field suppresses the crack driving force in the depth and encourages growth at the front surface. To exploit these tendencies, the user may wish to employ a combination of tension and bending stresses to produce the desired crack dimensions.

X1.2.2 A useful technique to measure crack shape evolution for a given starting notch and loading type is to intersperse fatigue marking cycles at a high stress ratio (*R*, see Terminology E1823) into an evolving surface crack. The marking bands on the fracture surface illustrate the shape evolution once the sample is broken open. This marking procedure should not be applied to samples intended for fracture testing.

X1.3 *Near-final Shape Initiation*—This method entails introducing a starting notch into the specimen that is very close to the desired final shape of the precrack, then allowing only limited fatigue crack growth to prevent the crack shape from evolving away from the desired shape. The starting notch should be very sharp and uniform, and should have the same shape as the desired precrack, but slightly smaller. Apply fatigue cycles to get the crack initiated around the entire perimeter of the notch and to grow the crack out to meet the minimum precrack extension requirements, but no further such that the shape is maintained. This methodology is useful for cracks with shapes away from the preferred propagation paths discussed above.

X2. USE OF POTENTIAL DIFFERENCE METHODS FOR MONITORING SURFACE CRACK EXTENSION

X2.1 *Method Summary*—Potential difference (PD) is a versatile, ubiquitous test method for the determination of crack initiation and growth in electrically conductive materials. The method operates on the principle that a crack in a current-carrying body acts as a discontinuity to the path of electrical conduction (**25**). This reduction in current-carrying area increases the electrical resistance of the body in the remaining ligament. Provided that a constant current is applied this translates into an increase in electrical potential difference (voltage) across the crack as the crack grows. A mathematical relationship, termed the calibration, can be developed to relate the empirical increase in measured potential difference to crack growth. A unique calibration exists for a given combination of specimen geometry and gauge configuration that is not a function of the material type, isothermal test temperature, or of the magnitude of the applied current. PD may be used for both specimen preparation (fatigue precracking) and testing (crack initiation and stable growth). By making in-situ, periodic electric potential (voltage) measurements at fixed points in the field (on the specimen surface), changes in crack length can be

estimated in real-time.

X2.1.1 A closed-form analytical solution for the relationship between voltage and crack length was established by Johnson (**26**) for the M(T) specimen; see also (**27**). Many adaptations of Johnson's equations are well known and accurate for calculating crack extension in two-dimensional symmetric geometries using PD change as input. The technique is well established for specimens having one characteristic crack dimension, such as the standard M(T), C(T), and SE(B) geometries (**28, 29**) for which very small crack length changes can be accurately measured. The same fundamental principle that makes PD a useful crack measurement technique for through crack geometries applies to monitoring of crack growth in surface crack specimens (**30**).

NOTE X2.1—Test Method E647 contains an annex with addition information regarding the potential difference method of crack monitoring.

X2.2 *Specimen Preparation*—The specimens to be instrumented for PD data acquisition require attachments for the current leads and voltage probe leads (typically two or more pairs). In plate or bar specimens, simple alligator or clothespin-type clips on the current leads clipped directly on the specimen ends are acceptable. For large plates or irregular geometries, current connection by some other means may be required. Precise location of the current leads is not critical, as long as a uniform current field is established in the vicinity of the crack plane and the attachment points do not move during the test. Symmetric locations relative to the crack plane and crack centerline are preferable.

X2.2.1 The voltage probe attachments and locations require increased attention. For readily weldable specimen materials, attaching probe wires using resistance spot welding works well. This attachment method allows the leads to be accurately located, uses little specimen space, and is relatively durable. The probe wires are typically of very small diameter, so a terminal strip near the specimen for transition from the probe wires to a more permanent connection into the data acquisition system is recommended. All probe wires should be shielded with appropriate insulating conduit and twisted together (if insulated) to shelter against stray thermoelectric effects. In order to mitigate the introduction of ground-loops, all devices used in the potential difference system, including test controllers, data-acquisition devices, power supplies, amplifiers, relays, and so forth, should be placed at a common electrical ground.

X2.3 *Equipment*—A computerized system for control and acquisition is strongly recommended. High gain, low noise amplification (typically 30 to 40 dB gain) is necessary to increase the measured PD data (typically on the order of 100 μV at the specimen) up to voltage levels that are readily recorded with digital data acquisition instrumentation. A suitable power supply capable of providing adequate constant current to the test specimen is also recommended.

X2.4 *Test Procedure*—Depending on the specimen size and configuration, the PD probe wires and other optional measurement transducers can be mounted either before or after placing the specimen in the test machine. This is mostly a matter of operator convenience, and the attachments are usually made after installing the specimen.

X2.4.1 It is important to consider the issue of electrical insulation from the test cell. Shunting of current through the test fixture will cause under prediction in the PD crack length measurements. Placing a thin layer of insulating tape (such as ultra-high molecular weight plastic) at the specimen contact points works well. This tape strain hardens, and after an initial loading, has only a small effect on system compliance and can be reused several times before replacement. One common practice to insure that there are no ground loops through the test cell is to measure the voltage across the crack before and after the specimen is mounted in the fixture. The two measurements will be equal if there are no appreciable current paths other than through the test specimen. A typical test cell usually has a resistance that is many orders of magnitude greater than the test specimen.

X2.4.2 The PD and mechanical test systems should be synchronized to facilitate test interpretation. Commonly, test machine data is sent to the PD data acquisition system to ensure synchronization.

X2.5 *Sources of Error*—The potential difference method relies on a precise relationship between voltage and crack length to relate an increase in potential difference to incremental crack growth. This model assumes that all changes in voltage are attributable to a change in crack size. There are, however, two other significant sources that can cause a measurable change in potential difference, namely, signal drift and plasticity.

X2.5.1 *Signal Drift*—Signal drift is most commonly associated with changes in temperature or changes within the PD test system. Temperature change causes the resistivity of the specimen material to change, which affects the measured voltage. System-level drift occurs when the response of system components such as amplifiers, relays, data-acquisition devices, or power supplies change over time. Both temperature and system drift produce apparent crack size changes that introduce error between the predicted and actual crack size.

X2.5.1.1 To compensate for these effects, the measured potential difference across the crack may be normalized by dividing this voltage by the voltage at some remote location on the specimen that is not influenced by local voltage changes caused by crack extension. Depending on specimen size, an ideal location may not exist that is satisfactorily remote from the perturbed electric field passing around the crack. In this case, the reference voltage should be measured on a separate reference specimen of the same material and geometry that is connected in series with the applied current. By measuring potential change across a section that does not contain a crack (but only material resistivity), the effect of temperature and system drift are strongly mitigated (**31**). The effects of temperature and system related drift are often not as critical to toughness testing as for tests which require a longer duration, such as fatigue crack growth rate testing. A more common perturbation, discussed below, is potential change due to plasticity.

X2.5.2 *Plasticity Influence*—When material at the crack tip deforms plastically, the local resistance of that material changes as well. This produces a change in the measured potential that is not related to actual crack extension. It is challenging to separate the two effects and often some trial and error with replicate specimens is required. One method of separating these effects is to plot the potential versus the CMOD. The two signals may plot as a straight line during plastic deformation without crack extension, and then deviate once crack extension begins (**32**). The effectiveness of this technique is somewhat compromised by the three dimensional nature of the surface crack geometry compared to more common two dimensional test samples. Furthermore, in monotonic tearing, surface crack extension generally will not occur evenly around the crack perimeter, but rather locally in symmetric points about the crack front. This further complicates the combined effects of plasticity and crack extension; however, the combination of potential difference and CMOD signals, once interpreted with supporting trial observations, will provide a useful method of identifying the initiation surface crack extension.

X3. USE OF DISPLACEMENT GAUGES AND INTERPRETATION OF THE FORCE-DISPLACEMENT RECORD

X3.1 Crack mouth opening displacement (CMOD) gauges are perhaps the easiest form of instrumentation to gain insight into the behavior of surface crack test specimens. They provide information on the amount of plasticity present around the crack and can aid with identification of crack tearing. CMOD methods are generally not as accurate for identifying the initiation of surface crack extension as are calibrated potential drop or acoustic emission methods; however, their simplicity can be favorable in the laboratory. For all but the smallest cracks, methods exist to attach a CMOD gauge. The gauge must track the opening displacement very close to the mouth of the crack to provide sufficient resolution. Fig. X3.1 illustrates methods for attaching the CMOD gauge to the crack face. For readily weldable materials, small clips can be spot welded on each side of the crack such that their tips track the CMOD, but they allow a typical fracture mechanics clip gauge to be attached. Another general approach adds a small notch or hole at the specimen surface which enables attachment of a miniature clip gauge to the front face of the specimen, directly in the crack mouth. Such miniature gauges are commercially available (**33**) or can be fabricated (**34**). Fig. X3.2(a)-(h) illustrate examples of miniature CMOD gauges and attachment holes that have been used successfully.

X3.2 Interpretation of the force versus CMOD record can provide meaningful information on crack behavior. The record contains three types of displacement information combined into a single CMOD value: elastic compliance corresponding to the initial crack geometry, plasticity, and the contributions of surface crack extension (ℓ) to CMOD. The difficulty arises in

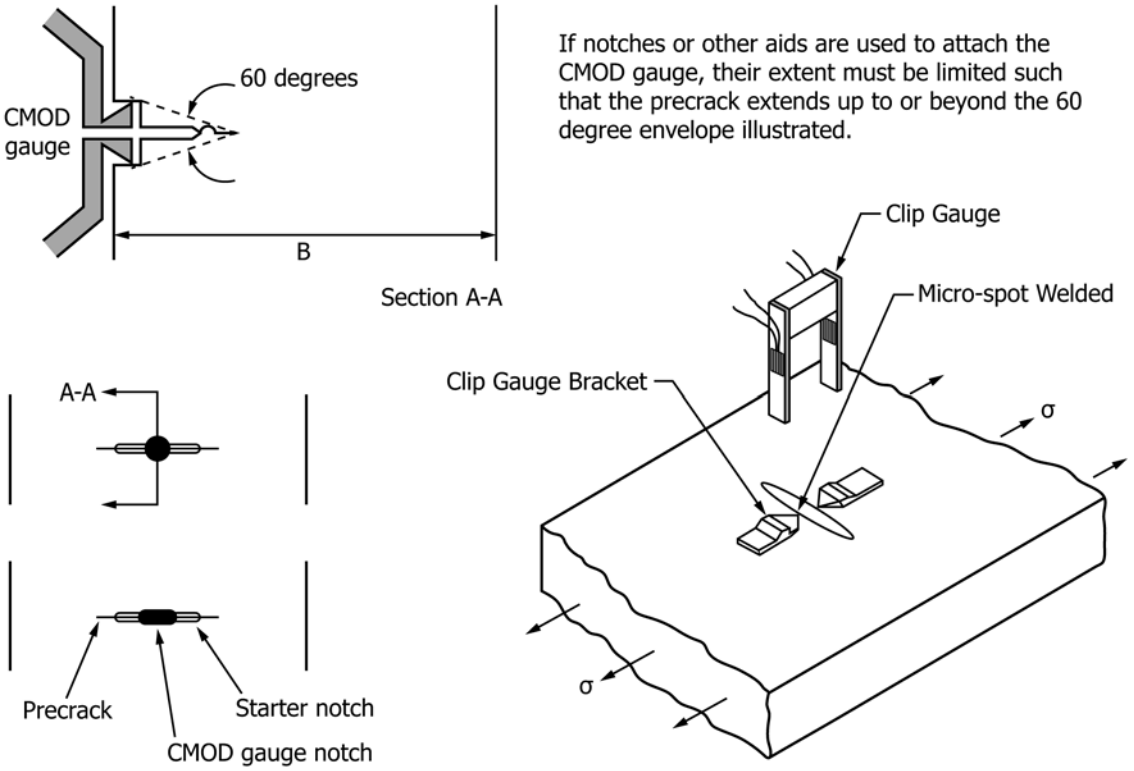

FIG. X3.1 Attachment methods for CMOD Gauges

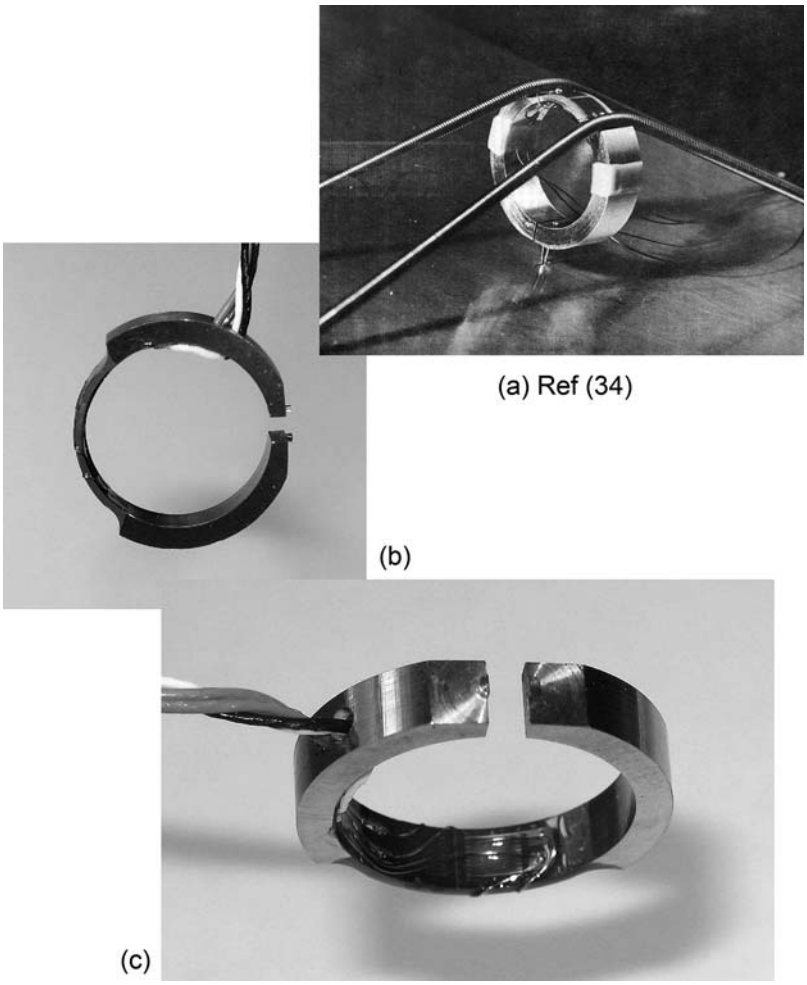

FIG. X3.2 Examples of CMOD Gauges and Attachments gauge designs courtesy of Ref. (33).

separating these contributions in a meaningful way. Fig. X3.3 provides a multi-step framework to use the CMOD trace as a guide to identify crack initiation; however, this method remains iterative and approximate.

X3.3 *Step 1*—(Not required, but recommended.) Test a precracked specimen directly to failure with the CMOD gauge. This test provides an estimate of the total deformation capability of the specimen.

X3.4 *Step 2*—Test a precracked specimen to a significant fraction of the total deformation capability. The point at which to unload this specimen may be judged in comparison to the test record (from Step 1) or to visual observation of specimen behavior, for example, visual evidence of crack extension at the surface. The unloading record should be kept for evaluation.

X3.5 *Step 3*—Once unloaded, the specimen is marked with fatigue or by other methods and then broken open. The force-CMOD trace may be analyzed as shown in Fig. X3.3 to correlate the three components of CMOD against the observed surface crack extension on the specimen. This insight should allow testing of additional specimens based on real-time review of the force-CMOD trace and to interrupt the test at an acceptable degree of surface crack extension (ℓ).

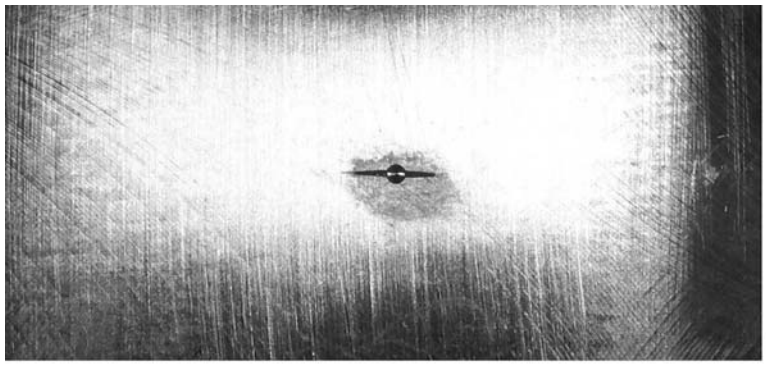

(d)

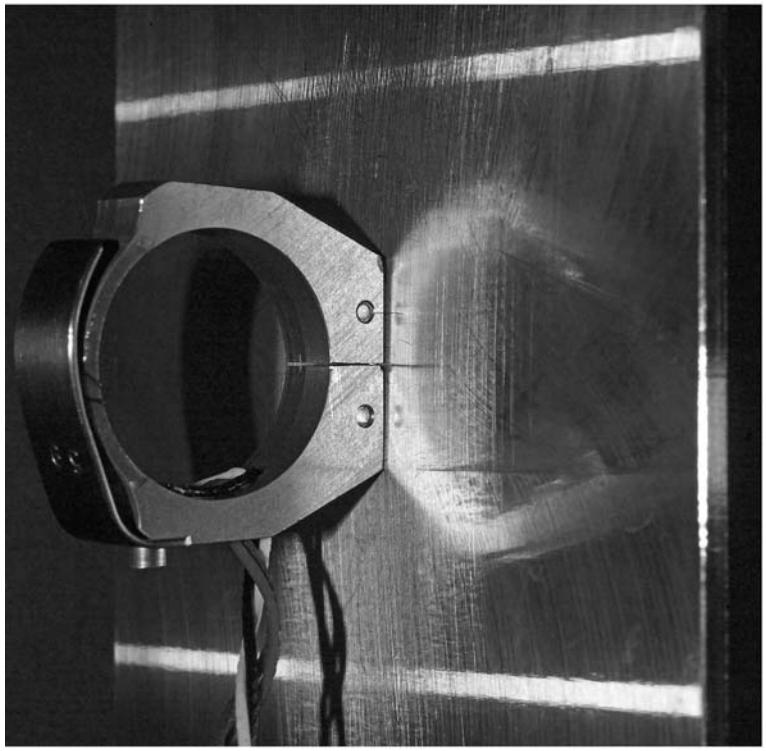

(e)

FIG. X3.2 Examples of CMOD Gauges and Attachments *(continued)*

(f)

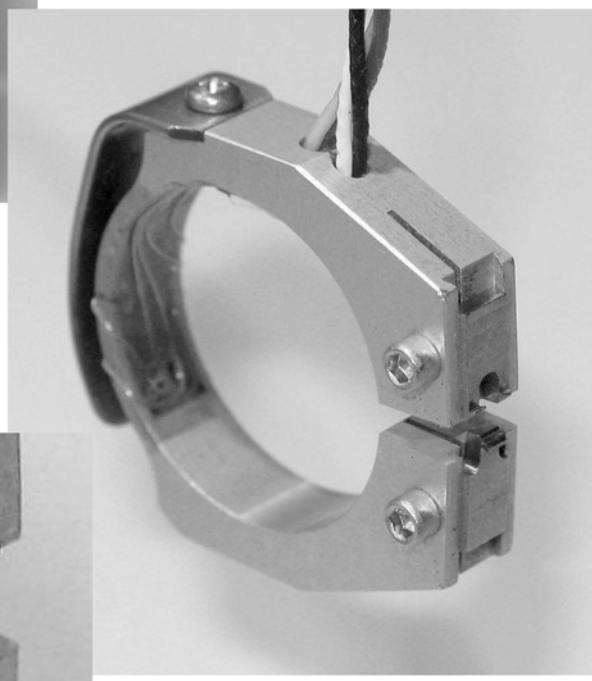

(g)

(h)

FIG. X3.2 Examples of CMOD Gauges and Attachments *(continued)*

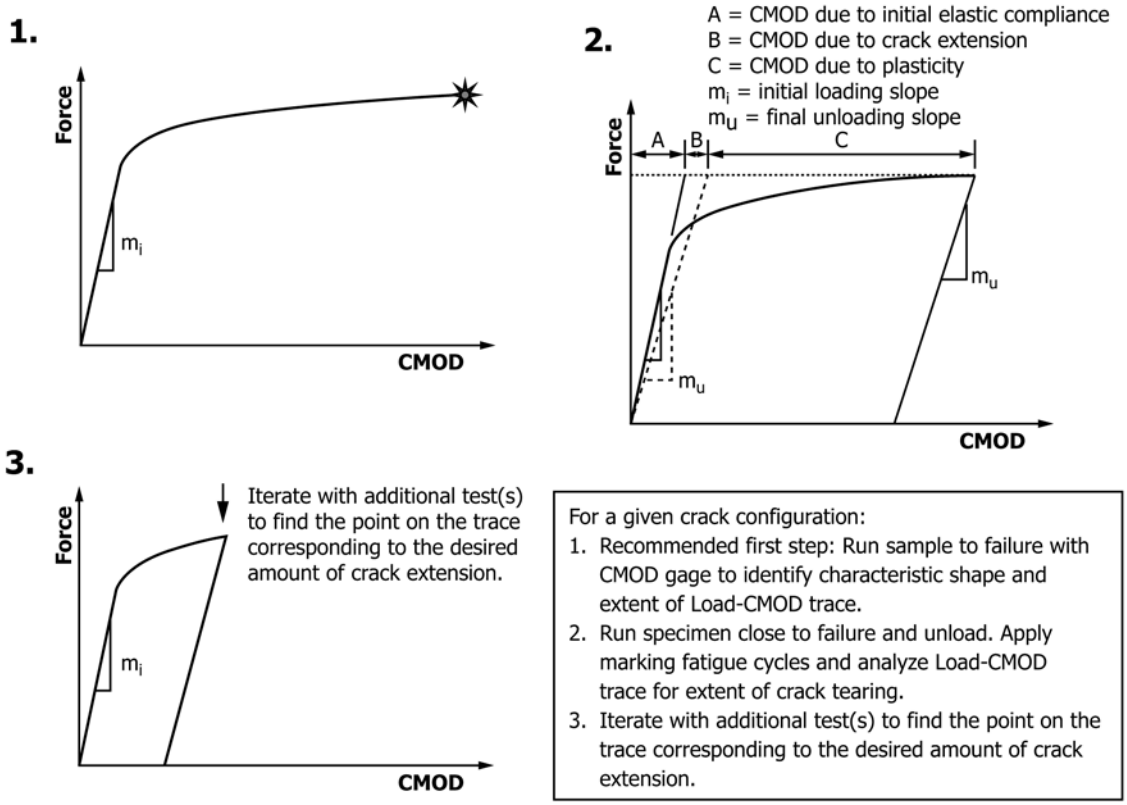

FIG. X3.3 Iterative Method for Identifying Crack Initiation Using CMOD data

X4. CONSTRAINT EFFECTS ON DUCTILE FRACTURE TOUGHNESS AND CRACK EXTENSION

X4.1 This test method encourages the development of constraint-correlated fracture toughness data from tests of surface crack specimens to support an improved understanding of surface crack data applied to structures. Surface crack tests and analysis of the results performed with this test method provide insight on constraint effects in the ductile fracture process for the material.

X4.2 The effects of constraint on strain and stress distributions in the crack-tip region are well understood from a continuum mechanics perspective (**6**, **7**, **8**, **17**, **35**). The realized effects of constraint on measured crack-initiation toughness vary with metallurgical-scale features of the material. These are governed by specific mechanisms of the fracture process operative in that material, at the test temperature and loading rate. These processes are generally far less well understood than the impact of constraint on the continuum strain-stress fields.

X4.3 The effects of constraint on the transgranular cleavage fracture mechanism in ferritic steels seem to have received the most attention and are arguably the most well understood, see review article (**36**). Ductile fracture—the focus of this test method—varies widely in the details of micromechanical separation processes; therefore predicting the effects of constraint on these fracture processes is determined here by direct experimentation and forms a key motivation for inclusion of quantified constraint measures in this test method.

X4.4 Crack-tip plasticity governs the development of constraint effects due to the heightened material contractions in the plastic region, together with equilibrium stresses that develop when linear-elastic material restrains the plastic deformation. For materials with linear-elastic behavior at the crack tip, constraint as quantified by the elastic *T*-stress, for example, has a negligible effect on crack-tip fields over distances at which the fracture separation processes occur. Fracture tests show much smaller or no effects of specimen geometry and loading (tension vs. bending) compared to those generally observed in ductile metals considered in this practice. For example, the work in (**37**) examines a ceramic material tested in geometries of widely varying constraint, yet all yield the same value of toughness. These tests were developed in support of Test Methods C1421.

X4.5 For more common metallic structural materials with fatigue sharpened crack fronts, crack-tip plasticity develops at the earliest stage of loading, and constraint alters the crack-tip conditions at some level over the full fracture test. Fig. X4.1 illustrates the various consequences of constraint effects on toughness. Curve A shows a strong trend of increasing toughness and tearing resistance as initially high constraint conditions relax with the continued spread of plastic deformation. This type of increased toughness may be most illustrative of

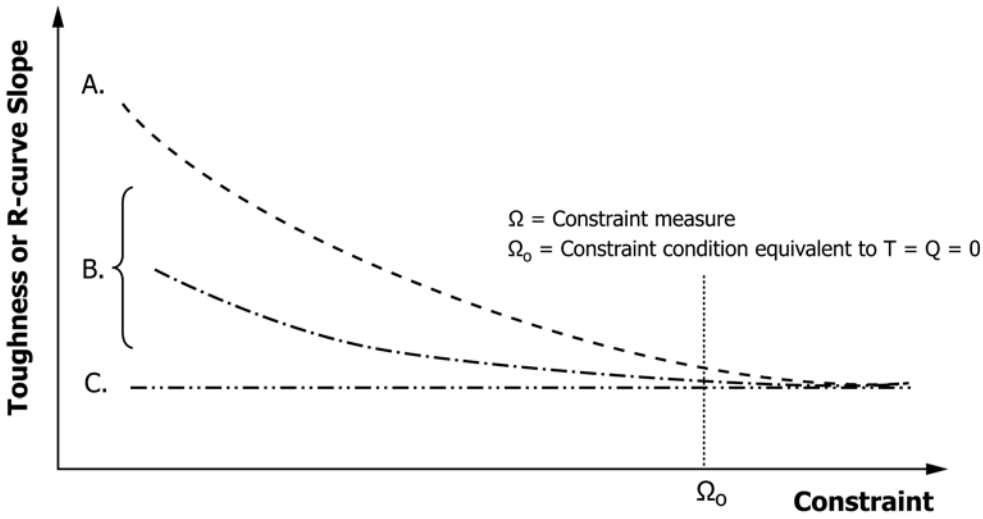

Potential patterns of behavior in the Toughness vs. Constraint locus:

A. Fracture processes dominated by stress fields (e.g. cleavage) show strong effects as lower constraint conditions have strong effects on crack tip stress fields.

B. Fracture processes which are a mixture of stress and strain influences (e.g. ductile fracture due to void growth) may have a broader range of response, but generally show an increase in toughness and R-curve slope with decreasing constraint.

C. Fracture processes which occur with vanishingly small crack tip plasticity exhibit no constraint dependence. Fracture toughness results are independent of specimen geometry.

FIG. X4.1 Expected Behaviors in the Toughness vs. Constraint Locus

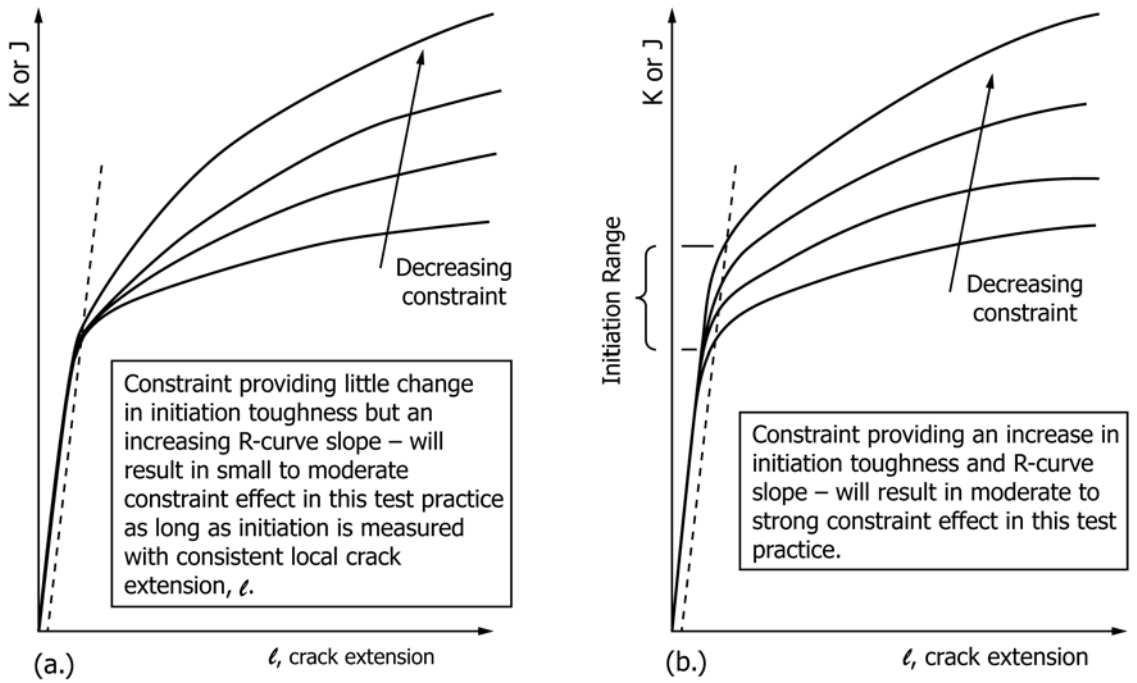

FIG. X4.2 (a) and (b) – Potential effects of toughness on crack initiation and growth from a resistance curve (R-curve) perspective: (a) little effect on initiation, more effect on R-curve slope, (b) constraint effects on both initiation and R-curve slope. This practice focuses on quantifying constraint effects on crack initiation.

constraint loss effects on materials that fracture with a cleavage mechanism. The strong dependence of the cleavage process on the level of tensile stresses in the near-tip region magnifies the toughness sensitivity to constraint loss. Decreasing constraint, for example, in a T-stress < 0 configuration, has a dramatic effect on lowering the opening-mode stress and mean stress, and thus has a strong effect on values of measured cleavage toughness, see (**38**) for example.

X4.6 Curve B of Fig. X4.1 illustrates the expected constraint effects observed in testing materials that fracture with a ductile (tearing) process (**1**). This test method focuses on testing of materials with fracture properties characterized by Curve B. Ductile fracture mechanisms (for example, void growth) generally reflect a combination of stress and strain influences. Tests exhibit a trend of increasing measured toughness in geometries with decreasing constraint. The constraint effects are likely to be less pronounced compared to materials with stress-based cleavage fracture. Some materials may exhibit a weak or essentially no impact of constraint loss on toughness, as Curve C illustrates.

X4.7 For the majority of structural metals tested successfully under this test method, the constraint effects are expected to generally follow the behavior indicated by Curve B of Fig. X4.1. Within this regime, constraint effects on fracture toughness appear primarily in two ways: *(1)* constraint may have little impact on the measured toughness value at crack initiation, but a significant and measurable impact on the (stable) tearing resistance curve (*R*-curve); or *(2)* constraint may affect both initiation and continued stable crack growth. Fig. X4.2 illustrates these two behaviors. If the material has little constraint dependence on initiation, and the tests are run with careful attention to a consistent measure of surface crack extension (ℓ) to avoid *R*-curve effects, then the resulting toughness-constraint locus will be relatively "flat". However, if the material exhibits a range of crack initiation values as constraint varies, then the toughness-constraint locus will have an increasing trend with decreasing constraint as shown by Curve B. Examples of these effects are shown in (**3, 4**).

X5. BACKGROUND REFERENCES

INTRODUCTION

The background references included here form the technical basis for the test and analysis methods in this test method. These background references are not cited in the text of this test method.

X5.1 Fundamentals of Crack-Tip Fields

Williams, M.L., "On the stress distribution at the base of a stationary crack," Journal of Applied Mechanics,Vol. 24, 1957, pp. 109-114.

Rice, J., Rosengren, G. "Plane strain deformation near a crack in a power law hardening material," Journal of the Mechanics and Physics of Solids, 16, 1968, pp. 1-12.

Hutchinson, J., "Singular behavior at the end of a tensile crack in a hardening material," Journal of the Mechanics and Physics of Solids," 16, 1968, pp. 13-31.

N. Levy, P. V. Marcal and J. R. Rice, "Progress in Three-Dimensional Elastic-Plastic Stress Analysis for Fracture Mechanics", Nuclear Engineering and Design, 17, 1971, pp. 64-75.

Rice, J., "Limitations to the small scale yielding approximation for crack tip plasticity," Journal of the Mechanics and Physics of Solids, 22, 1974, pp. 17-26.

Parks, D., Wang, Y., "Elastic-plastic analysis of part-through surface cracks," Analytical, Numerical, and Experimental Aspects of Three Dimensional Fracture Processes, A.J. Rosakis, K.Ravi- Chandar, and Y. Rajapakse, Eds., ASME AMD vol. 91. ASME, New York, 1988, pp. 19-32.

Sharma, S., Aravas, N. " Determination of higher-order terms in asymptotic elastoplastic crack tip solutions," Journal of the Mechanics and Physics of Solids, 39, No. 8, 1991, pp. 1043-1072.

Shum, D., "Effects of 3-D transverse constraint on the evolution of in-plane Q-stress," ASTM Special Technical Publication, STP 1256, 1995, pp. 178-195.

Kim, Y., Zhu, X., Chao, Y., "Quantification of constraint on elastic-plastic 3D crack front by the JA2 three-term solution," Engineering Fracture Mechanics, 68 (2001) 895-914.

X5.2 Methods and Solutions for Surface Cracks

Swedlow, J., Ed., The Surface Crack: Physical Problems and Computational Solutions, Winter Annual Meeting of the ASME, ASME, New York, 1972.

Rice , J., Levy, N. "The part-through surface crack in an elastic plate", Journal of Applied Mechanics, 39, 1972, pp. 185-194.

Sham, T., "The determination of the elastic T-term using higher order weight functions," International Journal of Fracture, 48, 1991, pp. 81-102.

Wang, Y., Parks, D., "Evaluation of the elastic T-stress in surface-cracked plates using the linespring method," International Journal of Fracture, 56, 1992, pp. 25-40.

Nakamura, T., Parks, D., "Determination of elastic T-stress along three-dimensional crack fronts using an interaction integral," International Journal of Solids and Structures, Vol. 29, No. 13, 1992, pp. 1597-1611.

Raju, I., Newman, J., and Atluri, S., "Crack mouth displacements for semi-elliptical surface cracks subjected to remote tension and bending loads," ASTM Special Technical Publication, STP 1131, 1992, pp. 19-28.

Sherry, A., France, C., Goldthorpe, M., "Compendium of T-stress solutions for two and three dimensional cracked geometries," Fatigue Fracture of Engineering Materials & Structures, 18 1995, pp. 141-155.

Wang, X., Lambert, S., "Stress intensity factors for low aspect ratio semi-elliptical surface cracks in finite thickness plates subjected to non-uniform stresses," Engineering Fracture Mechanics, 51, 1995, pp. 517-532.

Kim, Y., Shim, D., Choi, J., Kim, Y., "Approximate J estimates for tension-loaded plates with semi-elliptical surface cracks," Engineering Fracture Mechanics, 69, 2002, pp. 1447-1463.

Lei, Y., "J-integral and limit load analysis of semi-elliptical surface cracks in plates under tension," International Journal of Pressure Vessels and Piping, 81, 2004, pp. 21-30.

Wang, X., "Fully plastic J-integral solutions for surface cracked plates under biaxial loading," Engineering Fracture Mechanics, 73, 2006, pp. 1581-1595.

X5.3 **Experimental Methods and Results for Ductile Initiation and Continued Tearing**

Yen, C., PendleBerry, S., "Technique for making shallow cracks in sheet metals," Materials Research and Standards, 1962, pp. 913-916.

Corn, D., "A study of cracking techniques for obtaining partial thickness cracks of preselected depths and shapes," Engineering Fracture Mechanics, 3, 1971, pp. 45-52.

Orange, T. , "Fracture testing with surface crack specimens," Journal of Testing and Evaluation, 3, 1975, pp. 335-342.

Pierce, W. , Shannon, J. , "surface crack shape change in bending fatigue using an inexpensive resonant fatiguing apparatus," Journal of Testing and Evaluation, 6, 1978, pp. 183-188.

Schwartzberg, F., Toth, C., King, R., Todd, P., "Definition of mutually optimum NDI and proof test criteria for 2219 aluminum pressure vessels, Volume II – optimization and fracture studies," NASA CR-135446, 1979.

Joyce, J., Ernst, H. and Paris, P., "Direct evaluation of J-resistance curves from load displacement records," Fracture Mechanics: 12th Conference, ASTM STP 700, 1980, pg. 222.

Venkatasubramanian, T., Unvala, B., "An AC Potential drop system for monitoring crack length," Journal of Physics E: Scientific Instruments, 17, 1984.

Wang, Y., Parks, D., Lloyd, W., Reuter, W., Epstein, J., "Elastic-plastic deformation in surface cracked plates: experimental and numerical analysis," Journal of Applied Mechanics, 58, 1991, pp. 895-903.

Joyce, J. (Ed), "Elastic-plastic fracture test methods: the user's experience," ASTM STP 1114, 1991.

McCabe, D., Ernst, H., Newman, J., "Application of elastic and elastic-plastic fracture mechanics methods to surface flaws," ASTM Special Technical Publication, STP 1131, 1992, pp. 495-518.

Faleskog, J., "Effects of local constraint along three-dimensional crack fronts – a numerical and experimental investigation," Journal of the Mechanics and Physics of Solids, 43, 1995, pp. 447- 493.

Joyce, J. "Manual on elastic-plastic fracture: laboratory test procedures," ASTM International, 1996, ISBN-13: 978-0803120693.

Chao, Y., Reuter, W., "Fracture of surface cracks loaded in bending," ASTM Special Technical Publication, STP 1321, 1997.

Reuter, W.G., Newman, J.C.., Macdonald, B.D., Powell, S.R., "Fracture criteria for surface cracks in brittle materials," ASTM Special Technical Publication, STP 12007, 1994.

Zhu, X., Jang, S., "J-R curves corrected by load-independent constraint parameter in ductile crack growth," Engineering Fracture Mechanic , 68, 2001, pp. 285-301.

Christopher, T., Sankaranarayanasamy, K., Nageswara Rao, B., "Correlating cryogenic fracture strength using a modified two-parameter method," Engineering Fracture Mechanics,72, 2005, pp. 475-490.

Shepic, John A., Mechanical Metallurgist, 14031 W Exposition Dr., Lakewood, CO 80228-2321.

X5.4 **Computational Models for Initiation of Ductile Tearing and *R*-curves**

Xia, L. Shih, F., "Ductile crack growth-I. A numerical study using computational cells with microstructurally- based length scales, Journal of the Mechanics and Physics of Solids, 43, 1995, pp. 233- 259.

Xia, L. Shih, F., "Ductile crack growth-II. Void nucleation and geometry effects on macroscopic fracture behavior, Journal of the Mechanics and Physics of Solids, 43, 1995, pp. 1953-1981

Gao, X., Faleskog, J., Shih, F., "Cell model for nonlinear fracture analysis-I. Micromechanics calibration," International Journal of Fracture, 89, 1998, pp. 355-373.

Gao, X., Faleskog, J., Shih, F., "Cell model for nonlinear fracture analysis-II. Fracture-process calibration and verification," International Journal of Fracture, 89, 1998, pp. 375-398.

Gao, X., Faleskog, J., Shih, F., Dodds, R., "Ductile tearing in part-through cracks: experiments and cell-model predictions," Engineering Fracture Mechanics, 59, 1998, pp. 761-777.

Ruggieri, C., Panontin, T., Dodds, R. "Numerical modeling of ductile crack growth in 3-D using computational cell elements" International Journal of Fracture, 82, 1996, pp. 67-95.

Dawicke, D., Newman, J., "Residual strength predictions for multiple site damage cracking using a three-dimensional finite element analysis and a CTOA criterion," ASTM Special Technical Publication, STP 1332, 1997, pp. 815-829.

Gullerud, A., Dodds, R., Hampton, R., Dawicke, D., "Three-dimensional modeling of ductile crack growth in thin sheet metals: computational aspects and validation," Engineering Fracture Mechanics, 63, 1999, pp. 347-374.

Roy, Y., Dodds, R., "Simulation of ductile crack growth in thin aluminum panels using 3-D surface cohesive elements," International Journal of Fracture, 110, 2001, pp. 21-45.

X5.5 **Quantification of Constraint on Ductile Initiation and *R*-Curves**

McMeeking, R., Parks, D. "On criteria for J-dominance of crack tip fields in large-scale yielding," ASTM STP 668, 1979, pp.

Shih, F., "J-dominance under plane strain fully plastic conditions: the edge crack panel subject to combined tension and bending," International Journal of Fracture, 29, 1985, pp.73-84.

Sumpter, J., Hancock, J., "Shallow crack toughness of HY80 welds: An analysis based on Tstress," International Journal of Pressure Vessel & Piping, 45, 1991, pp. 207-221.

Newman, J., Crews, J., Bigelow, C., Dawicke, D., "Variations of a global constraint factor in cracked bodies under

tension and bending loads," ASTM Special Technical Publication, STP 1244, 1995, pp. 21-42.

Franco, C., Gilles, P., Eripret, C., and Nallet, S., "Constraint Effects on the Upper Shelf in Cracked Welded Specimens," ASTM Special Technical Publication, STP 1244, 1995.

O'Dowd, N., "Applications of two parameter approaches in elastic-plastic fracture mechanics," Engineering Fracture Mechanics, 52, 1995, pp. 445-465.

Hancock, J., Nekkal, A., "The application of constraint based fracture mechanics to engineering structures," Nuclear Engineering and Design, 184, 1998, pp. 77-88.

Ranestad, O., Zhang, Z.L., Thaulow, C., "An engineering method for constraint based fracture assessment of welded structural components with surface cracks," Engineering Fracture Mechanics, 63, 1999, pp. 653-674.

Thaulow, C., Zhang, Z., Hauge, M., Burget, W., Memhard, D., "Constraint effects on crack tip stress fields for cracks located at the fusion line of weldments," Computational Materials Science, 15, 1999, pp. 275-284.

Thaulow, C., Hauge, M., Zhang, Z., Ranestad, Ø., Fattorini, F., "On the interrelationship between fracture toughness and material mismatch for cracks located at the fusion line of weldments," Engineering Fracture Mechanics, 64, 1999, pp. 367-382.

Laukkanen, A., Nevasmaa, P., Ehrnsten, U., Rintamaa, R., "Characteristics relevant to ductile failure of bimetallic welds and evaluation of transferability of fracture properties," Nuclear Engineering and Design, 237, 2007, pp. 1-15.

Chao, Y., Zhu, X., "Constraint-modified J-R curves and its application to ductile crack growth," International Journal of Fracture, 106, 2000, pp. 1135-1160.

Joyce, J., Tregoning, R., "Development of consistent size criteria for ASTM combined fracture mechanics standards," ASTM Special Technical Publication, STP 1360, 2000, pp. 357-376.

Wang, Y., Reuter, W., Newman, J., "Analysis of brittle fracture in surface cracked plates using constraint-corrected stress fields," ASTM Special Technical Publication, STP 1417, 2002.

Liu, S., Chao, Y., "Variation of fracture toughness with constraint," International Journal of Fracture, 124, 2003 pp. 113-117.

Wallin, K., "Critical assessment of the standard ASTM E 399," ASTM Special Technical Publication, STP 1461, 2004.

Sherry, A., Wilkes, M., Beardsmore, D., Lidbury, D., "Material constraint parameters for the assessment of shallow defects in structural components-Part I: Parameter Solutions," Engineering Fracture Mechanics, 72, 2005, pp. 2373-2395.

Sherry, A., Hooten, D., Beardsmore, D., Lidbury, D., "Material constraint parameters for the assessment of shallow defects in structural components-Part II: Constraint-based assessment of shallow defects," Engineering Fracture Mechanics, 72, 2005, pp. 2396-2415.

Saxena, A., "Role of nonlinear fracture mechanics in assessing fracture and crack growth in welds," Engineering Fracture Mechanics, 74, 2007, 821-838.

REFERENCES

(1) Joyce, J. A., Link, R. E., Effects of constraint on upper-shelf toughness. *ASTM Special Technical Publication*. 1995;STP 1256:142-177.

(2) Shih, C. F., O'Dowd, N. P., Kirk, M. T., A framework for quantifying crack-tip constraint. *ASTM Special Technical Publication*. 1993;STP 1171:2-20.

(3) Hancock, J., Reuter, W., Parks, D. M., Constraint and toughness parameterized by T. *ASTM Special Technical Publication*. 1993;STP 1171:21-40.

(4) Joyce, J. A., Link, R. E., Application of two-parameter, elastic-plastic fracture mechanics to the analysis of structures. *Engineering Fracture Mechanics*. 1997;57:431-446.

(5) Shih, C. F., German, M. D., Requirements for a one-parameter characterization of crack-tip fields by the HRR singularity. *International Journal of Fracture*. 1981;17:27-43.

(6) Larsson, S., Carlsson, A., Influence of non-singular stress terms and specimen geometry on small-scale yielding at crack tips in elastic-plastic materials. *Journal of the Mechanics and Physics of Solids*. 1973;21:263-277.

(7) Leevers, P., Radon, J., Inherent stress biaxiality in various fracture fracture specimen geometries. *International Journal of Fracture*. 1982;19:311-325.

(8) Wang, Y., On the two parameter characgterization of elastic-plastic crack-front fields in surface cracks. *ASTM Special Technical Publication*. 1993;STP1171:120-138.

(9) O'Dowd, N. P., Shih, C. F., Family of crack-tip fields characterized by a triaxiality parameter – I. Structure of the field. *Journal of the Mechanics and Physics of Solids*. 1991;39:555-567.

(10) O'Dowd, N. P., Shih, C. F., Family of crack-tip fields characterized by a triaxiality parameter-II. Fracture applications. *Journal of the Mechanics and Physics of Solids*. 1992;40:939-963.

(11) Brocks, W., Schmitt, W., The second parameter in J-R curves: constraint or triaxiality. *ASTM Special Technical Publication*. 1995;STP1244:445-465.

(12) Yuan, H., Brocks, W., Quantification of constraint fields in elastic-plastic crack front fields. *Journal of the Mechanics and Physics of Solids*. 1998;46:219-241.

(13) Newman Jr, J. C., Bigelow, C. A., Shivakumar, K. N., Three-dimensional elastic-plastic finite-element analyses of constraint variations in cracked bodies. *Engineering Fracture Mechanics*. 1993;46:1-13.

(14) Leach, A. M., Daniewicz, S. R., Newman Jr, J. C., A new constraint based fracture criterion for surface cracks. *Engineering Fracture Mechanics*. 2007;74:1233-1242.

(15) *API 579, Recommended Practice 579-1 / ASME FFS-1, Fitness-For-Service*. 2nd Edition ed: American Petroleum Institute; 2007.

(16) *BS 7910, Guide to methods for assessing the acceptability of flaws in metallic structures*. British Standards Institution; 2005.

(17) Wang, Y., Parks, D. M., Limits of J-T characterization of elastic-plastic crack-tip fields. *ASTM Special Technical Publication*. 1995;STP1244:43-67.

(18) Reuter, W. G., Elfer, N., Hull, D., Newman Jr, J. C., Munz, D., Panontin, T. L., Fracture toughness results and preliminary analysis for international cooperative test program on specimens containing surface cracks. *ASTM Special Technical Publication*. 1997;STP 1321.

(19) Newman Jr, J. C., Raju, I. S., Stress-intensity Factor Equations for Cracks in Three-Dimensional Finite Bodies Subjected to Tension and Bending Loads. *Computational Methods in the Mechanics of Fracture*. 1986;2:311-334.

(20) Newman Jr, J. C., Reuter, W. G., Aveline, C. R. J., Stress and Fracture Analyses of Semi-Elliptical Surface Cracks. *ASTM Special Technical Publication*. 2000;STP1360:403-423.

(21) Wang, X., Elastic T-stress solutions for semi-elliptical surface cracks in finite thickness plates. *Engineering Fracture Mechanics*. 2003;70:731-756.

(22) Wang, X., Bell, R., Elastic T-stress solutions for semi-elliptical surface cracks in finite thickness plates subject to non-uniform stress distributions. *Engineering Fracture Mechanics*. 2004;71:1477-1496.

(23) Wells, D. N., Allen, P. A., *Analytical Round Robin for Elastic-Plastic Analysis of Surface Cracked Plates: Phase I Results*. NASA MSFC; 2012. NASA/TM-2012-217456.

(24) Wu, S. X., Shape change of surface crack during fatigue growth. *Engineering Fracture Mechanics*. 1985;22(5):897-913.

(25) Barnett, W. J., Troiano, A. R., Crack propogation in hydrogen-induced brittle fracture of steel. *Journal of Metals*. 1957:486-494.

(26) Johnson, H. H., calibrating the Electric Potential Method for Studying Slow Crack Growth. *Materials Research and Standards*. 1965:442-445.

(27) Schwalbe, K. H. S., Hellmann, D., Application of electric potential method to crack length measurements using Johnson's formula. *Journal of Testing and Evaluation*. 1981;9(3):218-221.

(28) Aronson, G. H., Ritchie, R. O., Optimization of the electrical potential technique for crack growth monitoring in compact test pieces using finite element analysis. *Journal of Testing and Evaluation*. 1979;7(4):208-215.

(29) McKeighan, P. C., Smith, D. J., Determining the potential drop calibration of a fatigue crack growth specimen subject to limited experimental observations. *Journal of Testing and Evaluation*. 1994;22(4):291-301.

(30) Gangloff, R. P., Electrical potential monitoring of crack formation and subcritical growth from small defects. *Fatigue of Engineering Materials and Structures*. 1981;4(1):15-33.

(31) Donald, K. J., Ruschau, J., Direct Current Potential Difference Fatigue Crack Measurement Techniques. In: Marsh KJ, Ritchie RO, Smith RA, eds. *Fatigue Crack Measurements: Techniques and Applications*. Engineering Materials Advisory Services, LTD; 1990.

(32) Marschall, C. W., Held, P. R., Landow, M. P., Mincer, P. N., Use of direct-current electrical potential method to monitor large amounts of crack growth in highly ductile metals. *ASTM Special Technical Publication*. 1990;1074:581-593.

(33) Shepic, J. A., Mechanical Metallurgist, 14031 W. Exposition Dr., Lakewood, CO 80228 (USA).

(34) Schwartzberg, F., Toth, C., King, R., Todd, P., *Definition of mutually optimum NDI and proof test criteria for 2219 aluminum pressure vessels, Volume II – optimization and fracture studies*. NASA CR-135446; 1979.

(35) Du, Z., Hancock, J., The effect of non-singular stresses on the crack-tip constraint. *Journal of the Mechanics and Physics of Solids*. 1991;39:555-567.

(36) Pineau, A., Development of the Local Approach to Fracture over the Past 25 years: Theory and Applications. *International Journal of Fracture*. 2006;138:139-166.

(37) Quinn, G. D., Xu, K., Salem, J. A., Swab, J. J., SRM 2100: the world's first fracture toughness reference material. In: Bradt RC, Munz D, Sakai M, White KW, eds. *Fracture Mechanics of Glasses and Ceramics*. Vol 14: Kluwer/Plenum, NY; 2005:499-530.

(38) Ruggieri, C., Dodds, R. H. J., Wallin, K., Constraint Effects on Reference Temperature, To, for Ferritic Steels in the Transition Region. *Engineering Fracture Mechanics*. 1998;60:19-37.